UNIVERSITY OF CALIFORNIA,
IRVINE

Weak and strong binding states and tubulin C terminal tails affect intracellular transport

DISSERTATION

submitted in partial satisfaction of the requirements
for the degree of

DOCTOR OF PHILOSOPHY

in Mathematical, Computational and Systems Biology

by

Trini Nguyen

Dissertation Committee:
Assistant Professor Chris Miles, Chair
Professor Steve Gross
Professor Lee Bardwell
Associate Professor Michelle Digman

2024

DEDICATION

To my family: stop asking me when I will defend.
To Nathan Khai Nguyen: there, your name is now in a book.

TABLE OF CONTENTS

LIST OF FIGURES

LIST OF TABLES

ACKNOWLEDGMENTS

Chapter 2 is reprinted and adapted with permission from Trini Nguyen, Babu Reddy, Steven Gross, and Chris Miles. Chapter 3 is reprinted and adapted with permission from Trini Nguyen, Steven Gross, and Chris Miles. These authors thank Brennan Sprinkle for helpful discussions about Brownian hydrodynamics. Financial support was granted by various sources over the years: the UCI Diversity Recruitment Fellowship, the NSF-Simons Center for Multiscale Cellfate Research Fellowship, the National Science Foundation Graduate Research Fellowship Program, and the UCI Graduate Dean Dissertation Fellowship.

Some figures were made with icons by Servier `https://smart.servier.com/`, which is licensed under CC-BY 3.0 Unported. This work utilized the infrastructure for high-performance and high-throughput computing, research data storage and analysis, and scientific software tool integration built, operated, and updated by the Research Cyberinfrastructure Center (RCIC) at the University of California, Irvine (UCI).The RCIC provides cluster-based systems, application software, and scalable storage to directly support the UCI research community. `https://rcic.uci.edu`

VITA

Trini Nguyen

EDUCATION

Ph.D. in Mathematical, Computational and Systems Biology **2024**

University of California, Irvine *Irvine, CA*

Bachelor of Arts in Mathematics **2018**

California State University, Fullerton *Fullerton, CA*

RESEARCH EXPERIENCE

Graduate Student Researcher **2018–2024**

University of California, Irvine *Irvine, California*

Undergraduate Student Researcher **2016–2018**

California State University, Fullerton *Fullerton, California*

Summer Research Intern **2017**

University of California, San Diego *La Jolla, California*

TEACHING EXPERIENCE

Developmental Biology Teaching Assistant **2024**

University of California, Irvine *Irvine, CA*

MCSB Bootcamp Tutor & Teaching Assistant **2019–2021**

University of California, Irvine *Irvine, CA*

Math Teaching Assistant **2021**

The California State Summer School for Math & Science *Irvine, CA*

Systems Biology Foundations Short Course Teaching Assistant **2020**

University of California, Irvine *Irvine, CA*

REFEREED JOURNAL PUBLICATIONS

Competition between physical search and a weak-to-strong transition limits kinesin binding times **2024**

PLOS Computational Biology

Computational modeling reveals a catch-and-guide interaction between kinesin-1 and tubulin C terminal tails **2024**

Traffic (tentative)

ABSTRACT OF THE DISSERTATION

Weak and strong binding states and tubulin C terminal tails affect intracellular transport

By

Trini Nguyen

Doctor of Philosophy in Mathematical, Computational and Systems Biology

University of California, Irvine, 2024

Assistant Professor Chris Miles, Chair

Intracellular transport is the process by which cargoes, such as organelles, travel to their needed locations within the cell in a timely manner via cytoskeletal filaments. This process involves the cargo that needs to be transported, motor proteins such as kinesin, and a filament, such as the microtubule. The process is broken down into several sub-processes, two of which are the focus in this study: the binding process (in which the cargo-motor protein ensemble binds to the microtubule) and processivity (where the cargo-motor ensemble walks on the microtubule). It is known which structures in the cell are used in intracellular transport, such as motor proteins, microtubules, and tubulin C terminal tails (CTTs); however, it is unclear how their properties affect the entire process. In this study, we use mathematical modeling and computational simulations to explain perplexing details of experimental data. Specifically, we show that motor diffusion alone cannot explain binding times measured from optical trap studies. Through computational analysis, we suggest that ADP release from the motor head may be an integral component of the binding process. We also propose the contribution CTTs provide to motor proteins processivity, where we believe CTTs help motor heads that are searching for microtubule binding sites by holding them near the microtubule, thus allowing for quicker steps. By combining modeling and simulations with experimental data, we can tune physical parameters that have the most potential of explaining the data, which in turns allow us a deeper understanding of intracellular transport.

Chapter 1

Introduction

For the cell to function correctly, its proteins, organelles, and other cargoes must travel efficiently to their intended destinations via a process called intracellular transport [33]. In this process, cargoes use molecular motors to travel on a cytoskeletal network within the cell (Figure 1.1). The process is a complex one, and the diverse and numerous components that are required for intracellular transport contribute to its complexity. Some of these components include subcellular cargoes, motor proteins, and filaments upon which the cargoes travel on [114]. Examples of subcellular cargoes that utilize this type of transport include mitochondria, lipid droplets, and vesicles, and they use motor proteins, such as kinesin, dynein, and myosin, to walk on cytoskeletal filaments such as microtubules and actin. Other proteins are also involved in intracellular transport, especially those that decorate the microtubule surface, such as tau and tubulin C terminal tails (CTTs) [33]. All of these components differ greatly in size, shape, and interactions with each other, which forces the cell to strictly regulate intracellular transport. The process has been very carefully studied, since transport malfunctions have been connected to neurodegenerative diseases, such as Parkinson's and Alzheimer's diseases [75, 117, 20]. However, it is still unclear how certain properties, such as physical factors and chemical interactions, of each of the structures involved in trans-

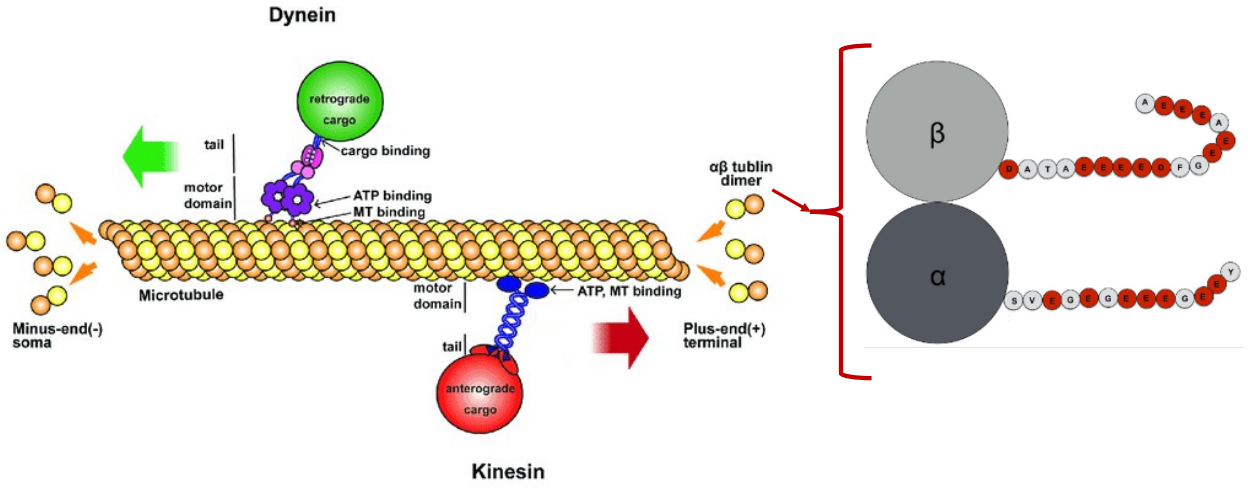

Figure 1.1: Intracellular Transport System. Cargoes can use motor proteins to travel one of two directions on the microtubule: they can use dynein to walk in the retrograde direction (towards the minus end of the microtubule) and kinesin for the anterograde direction (towards the plus end). The motor proteins primarily consist of two parts, the tail which binds to the cargo, and the motor domain which are used to bind to and walk on the microtubule. The motor must be in a specific state, such as being bound to ATP, to bind to the microtubule and walk on it. Microtubules consist of tubulin dimers, which consist of α and β tubulin monomers polymerizing together. Proteins on the microtubule control motor protein traffic, such as C terminal tails that protrude out of each tubulin monomer. Adapted from [36, 57].

port affect the overall process. This dissertation focuses on motor size, spacing between two proteins, and interactions between these proteins.

1.1 Microtubules and CTTs

Microtubules are formed when $\alpha\beta$-tubulin dimers polymerize together (Figure 1.1) [80]. In eukaryotic cells, microtubules consist of 13 protofilaments and are about 25 nm in diameter. These polymers can be as long as 50 μm, which allows for cargoes to travel long distances within the cell. Each tubulin monomer is about 8 nm long and contain a binding site for motor proteins to bind to and step on, so each motor step is also about 8 nm long. Microtubules are heavily decorated with proteins, and it is believed that these proteins

regulate motor protein traffic [102]. These proteins range in size and activity, in which some are longer than others and can either speed up the motor binding or unbinding from the microtubule. Thus, binding to the microtubule surface and walking along it are not straight-forward processes. One of the proteins that seem to regulate motor protein traffic on the microtubule are CTTs [80]. These negatively-charged tails extend from each tubulin monomer, where α CTTs are slightly shorter than β CTTs, but both are about 10 nm in length. It is not clear how CTTs contribute to motor processivity, but their interactions with motor proteins and structure are being heavily studied. For example, post-translational modifications are found to be highly complex on CTTs [46]. These modifications seem to be coordinated with motor protein function. Microtubules with less polyglutamylation, which occurs only on α CTTs, seem to result in lower motor binding events [61]. If α CTTs discourage binding, perhaps they are shorter than β CTTs to have a balance of bound motors versus unbound motors. Another example of a CTT study includes ends of microtubules that are near the soma of the neuron, which have detyrosinated CTTs, whereas the other end (where dynein-dynactin lands) have tyrosinated CTTs [46]. Thus, it is clear that CTTs use post-translational modifications to dictate how often and which motors can bind to the microtubule, but there remains many unknown details about CTTs. In further attempt to understand the purpose of CTTs, experiments that use subtilisin to remove CTTs from microtubules have been performed. In one of these studies, removal of the CTTs resulted in a significant decrease of KIF1A's (a member of the kinesin family) binding rate to the microtubule [61], although it is possible that too much subtilisin was used and the resulting damage to the microtubule may have not allowed for motor binding. Still, it seems that some CTTs may also help recruit motors to the microtubule. Removal of CTTs have also been seen to decrease both the run-length and velocity of motors [102]. It is not very obvious how CTTs can achieve both longer motor run-lengths *and* faster velocities on the microtubule. For example, it can be hypothesized that CTTs help motors by catching them as they fall off the microtubule, and this assistance would certainly extend motor run-lengths. However, it is

likely that merely catching the motors would slow them down, as it takes time for the motor to rebind to the microtubule after some diffusive search. Thus, the purpose of CTTs remain a mystery. However, as CTTs exist very closely to motor binding sites on microtubules [46], they are very much worth studying when attempting to understand intracellular transport. Chapter 3 of this dissertation focuses on possible CTT models that can explain the perplexing result seen in [102].

1.2 Kinesin Motor Protein and its Interactions with the Microtubule

Much research have been performed on kinesin motor proteins traveling on the microtubule [70, 86]. Kinesin motors consist of two heads (also known as the motor domain), which are used to perform stepping on the microtubule (Figure 1.1) [127]. Kinesins typically transport cargoes from the center of the cell to the periphery, known as the anterograde direction [7]. There are 14 known kinesin families, and each of these kinesins differ in organisms of which they exist, size, and movement patterns, among other properties [58]. This study focuses primarily on kinesin-1, which has been connected to several neurodegenerative diseases and have great clinical importance [91, 78, 119]. Thus, understanding their properties are very necessary. This kinesin protein is made up of both heavy and light chain molecules [44]. The cargo binds to the light chains via binding proteins, and the heavy chains make up the rest of the motor, including the two heads that connect to the long stalk with a short but flexible neck linker. Binding of the heads to the microtubule is dictated by ATP and ADP molecules (Figure 1.2). Each head has a separate binding site for the microtubule and for ATP. ADP release and ATP binding and hydrolysis all result in the neck linker turning the head to allow for microtubule binding. In fact, single-molecule studies have shown that ADP release is required for motor stepping [104]. The estimates of the rate of ADP release

vary greatly in the literature [26, 100, 101, 38, 41, 105, 29, 2], mainly due to the numerous types of kinesin studied and the disparity of the ADP release rate between two bound heads versus one bound head. It is also not clear whether the ADP release rate for stepping is the same for binding. Thus, there is still work that needs to be completed to understand the mechanisms that allow kinesin to bind to the microtubule.

Unbinding of the motor from the microtubule can be measured by experiments. In [79], the authors were able to measure the force required for myosin to detach from actin using optical tweezers, and a similar experimental setup can be used to measure kinesin unbinding forces. These types of experiments have also been used to observe processivity [64], and others have used high-resolution traces to measure run-length and velocities [53]. Thus, there are many experimental methods to study unbinding and organelle motion. Binding, however, is more difficult to study. In experiments, it is difficult to observe the moment the motor binds to the microtubule, which is not necessarily when it begins to walk on the microtubule. Nevertheless, there are still studies that attempt to study binding. A common finding of these studies is the observation of a weak bound state between the motor and the microtubule [45, 128, 21]. It is not clear what is limiting the motor to strongly bind to the microtubule from this weak bound state, but since ADP release is the rate-limiting step for kinesin walking [37], it could also be the rate-limiting step for kinesin initial binding. Chapter 2 explores this model of binding.

1.3 Current Understanding of the Binding Process

There is much to uncover about the specifics of the motor-microtubule binding process, and there has been attempts at clarifying this important process. Motors can either bind directly to the microtubule, or with the assistance from microtubule-associated proteins (MAPs) that decorate the microtubule surface [35]. For example, it has been found that

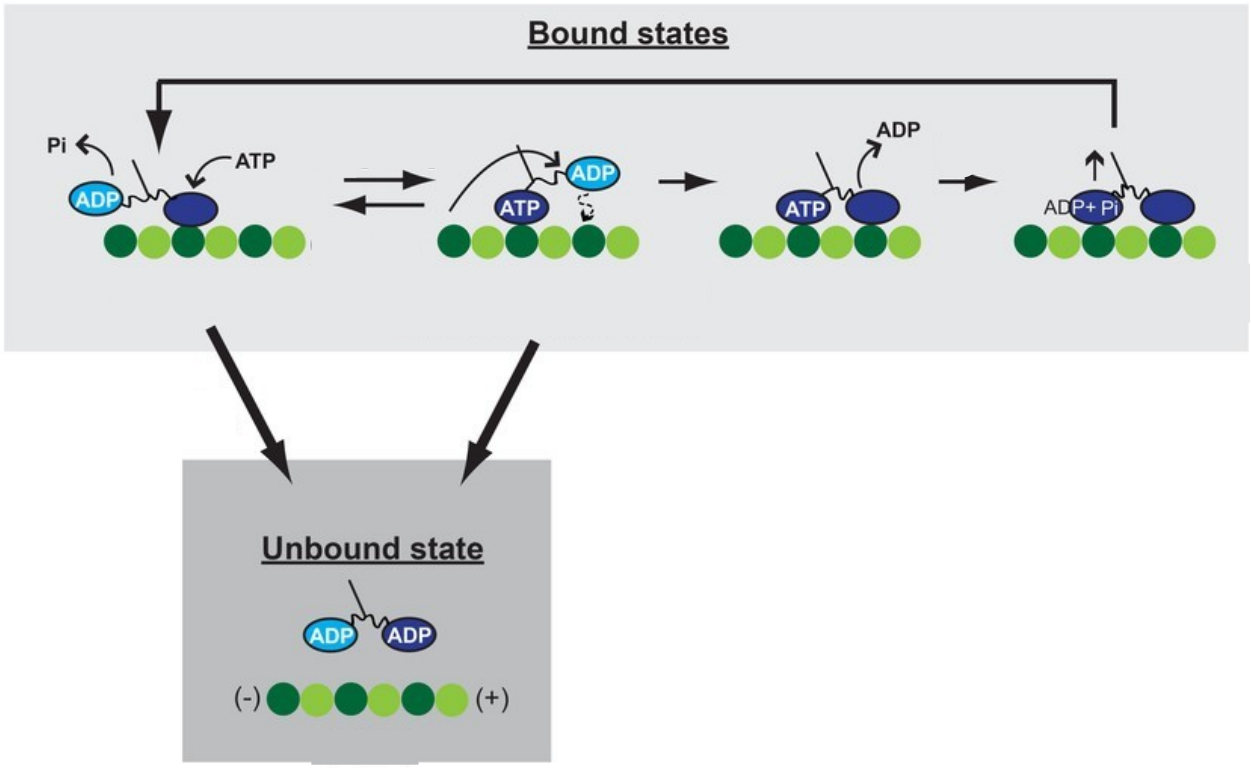

Figure 1.2: Kinesin Step Cycle. When a kinesin head steps on the microtubule and binds to it, ADP is released. This allows for ATP to be recruited to this leading head, which results in a neck linker conformation that turns the trailing head forward. The ATP-bound head then releases a phosphate group to become an ADP-bound head. This results in a weak affinity between that bound head and the microtubule, and the motor can unbind from the microtubule at this point. Adapted from [77].

MAP7 plays an important role in kinesin-1 recruitment to the microtubule [45]. Some proteins inhibit the motor from binding to the microtubule [48], but this inhibition can be relieved by other proteins, such as protein-γ1 and Jun N-terminal kinase-interacting protein 1, which bind to the motor instead of the microtubule [115]. It is not clear what signals these proteins to become activated at specific times, but the known system of this traffic is certainly impressive. Other elements that decorate the microtubule aside from MAPs are CTTs, but it is still difficult to understand how they affect motor binding. For example, there is evidence that suggests α CTTs decrease motor-microtubule binding rates, but β CTTs help with motor recruitment to the microtubule [102]. The two different types of CTTs are only different in length by about 4 nm [80]. It is difficult to hypothesize how these lengths can have completely different behaviors, so what other differences between these two CTTs result in their polarizing interactions with the motor? There are other observed mechanisms that the cell uses to control motor-microtubule binding. The microtubule itself can influence binding of motors through post-translational modifications, such as acetylation [90], which happens directly on the microtubule, not on its CTTs. The mechanism of post-translational modifications controlling motor binding is still not clear; perhaps the modifications change the charge of the microtubule binding site, making the affinity to motors stronger, or the modifications make CTTs longer (or shorter), which affects the motor's diffusive search time for the microtubule. Other post-translational modifications that affect motor-microtubule binding can happen on the motor, such as phosphorylation, and these modifications can change the orientation of the motor so that microtubule binding site on the motor domain becames more accessible to the microtubule and binding becomes easier [22]. It is possible that the kinesin's orientation is important for binding, and thus other conformational changes of kinesin should be studied, such as ADP release. Because there are so many factors that affect binding, there are many possible ways for binding to malfunction. Since binding is the very first step of intracellular transport, any malfunction in the binding process would disrupt the entire transport process. Thus, it is important to understand the complete details

of binding to find areas for neurodegenerative disease medicines and therapy improvement.

1.4 The Value of Computational Approaches in Intracellular Transport Studies

Experimental studies are valuable in measuring and observing cellular processes in real time; however, as much information is being uncovered about these processes, the realization of the limit of what we can observe is being manifested. For example, we cannot observe the specific details of binding, and we cannot disentangle between binding and the first walking step of a motor. We also cannot observe the specific details of the motor interacting with other proteins on the microtubule. However, computational models can help with these limitations. Computational models can be used in combination with experimental studies to relate subcellular phenomena to observed behaviors (Figure 1.3). For example, with analytical and numerical models, scientists can study the isolated effects of certain parameters, such as protein size and binding rates, that are difficult to control in experiments alone. [84] have done this analysis in which they used a Markov chain model to control the length of an actin filament and understand its effects on cargo travel speed. The ability to control protein size is valuable because they are a wide variety of proteins and each of them come in different sizes, so understanding the effect of size on a system can help biologists summarize the effects from numerous proteins. There are a variety of computational methods available to study intracellular transport, and these include stochastic models [124], where the effect of random noise is incorporated to reflect the range of effects that are observed in experiments. In intracellular transport studies, stochastic models typically simulate biophysical effects of a system [86], and these models are extremely helpful because they mimic known biological processes very closely. However, simulating biophysical effects, such as steric effects, can be very computationally expensive. Some stochastic models do not include biophysical effects,

such as the Gillespie algorithm [30], which generates possible solutions of stochastic equations with known reaction rates. Often times, Gillespie-styled simulations are computationally less expensive than biophysical simulations, but that is because less details are considered. Ideally, both types of studies should be done; rough estimates of unknown parameters can be easier obtained through less computationally expensive algorithms, but more computationally expensive algorithms can allow insight of effects of intricate details. There is also the issue of determining the entire set of biologically feasible parameters that allows these models to explain the data. Statistical algorithms can be used to address this issue. It seems that there is no singular method that can be used to holistically study intracellular transport. The projects in this dissertation employ many different methods to study intracellular transport: both experiments and computational methods. With respect to computational methods, this dissertation includes both computationally expensive analyses to understand a complicated experimental setup, and a less computationally expensive analysis to propose models of a simpler experimental setup. We also use statistical algorithms to further understand intracellular transport. By combining experimental data and theory, we can effectively understand the interactions between the motor protein and the microtubule.

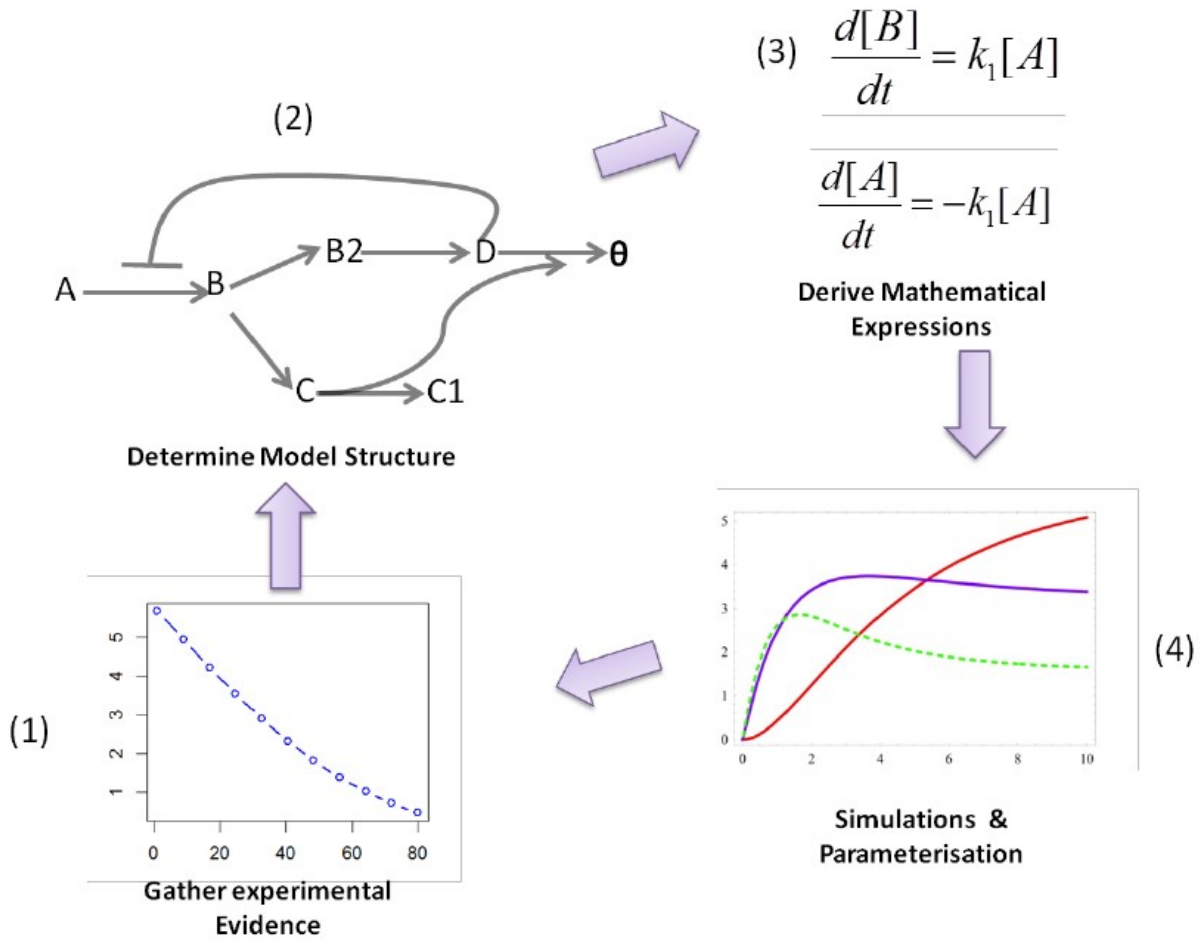

Figure 1.3: Combining Experimental Data with Theory. To effectively study biological processes, a variety of methods should be used. In computational biology, experimental data is typically gathered first. If this data is too perplexing and more experiments are not feasible or not efficient, then computational methods should be employed. An appropriate model should be hypothesized from the data. The model can then be translated into mathematics, and computer simulations of the mathematical model can provide more insight into the experimental data. Adapted from [16].

Chapter 2

Competition between physical search and a weak-to-strong transition rate limits kinesin binding times

2.1 Abstract

The self-organization of cells relies on the profound complexity of protein-protein interactions. Challenges in directly observing these events have hindered progress toward understanding their diverse behaviors. One notable example is the interaction between molecular motors and cytoskeletal systems that combine to perform a variety of cellular functions. In this work, we leverage theory and experiments to identify and quantify the rate-limiting mechanism of the initial association between a cargo-bound kinesin motor and a microtubule track. Recent advances in optical tweezers provide binding times for several lengths of kinesin motors trapped at varying distances from a microtubule, empowering the investigation of competing models. We first explore a diffusion-limited model of binding. Through Brown-

ian dynamics simulations and simulation-based inference, we find this simple diffusion model fails to explain the experimental binding times, but an extended model that accounts for the ADP state of the molecular motor agrees closely with the data, even under the scrutiny of penalizing for additional model complexity. We provide quantification of both kinetic rates and biophysical parameters underlying the proposed binding process. Our model suggests that a typical binding event is limited by ADP state rather than physical search. Lastly, we predict how these association rates can be modulated in distinct ways through variation of environmental concentrations and physical properties.

2.2 Introduction

Life depends on an immensely diverse and complex array of protein-protein interactions [96]. These interactions are richly regulated in both space and time (e.g., via post-translational modifications, fluctuating concentrations [67]) to modulate affinities, promiscuities, and sensitivities [97]. Understanding how these interactions are parameterized by both chemical and physical factors is broadly limited due to challenges in observing interaction events directly [111]. While predicting interactions from molecular structures (e.g., from molecular dynamics simulations) is an invaluable approach, these investigations still suffer from the same observational limitation in their validation [87].

One variety of such interactions of major importance across cellular function are those between molecular motors and cytoskeletal filaments. Cytoskeletal motors, specifically kinesin-microtubule assemblies, self-organize to perform a zoo of cellular behaviors, including the delivery of cargoes in intracellular transport [33], generation of forces to guide genetic material in mitosis [122, 110], and guiding of axonal growth [76]. Each of these wildly different behaviors is fundamentally achieved through molecular motors binding, stepping, and unbinding from cytoskeletal filaments [130]. Over the last several decades, advancements in

single-molecule experiments have revealed extensive details about the latter two components [79, 51, 98]. Stepping and unbinding are, in some sense, *downstream* of binding, suggesting clear merit in understanding the details underlying the process.

Pursuits toward understanding motor-cytoskeleton binding have been clouded by complications in disentangling the measurements from convolving factors. That is, one must specify exactly the notion of binding that is being measured. To do so, consider the full process of self-assembly. Initially, a freely diffusing motor associates with a cargo, the motor-cargo complex then diffuses into close proximity to a cytoskeletal filament, and then the first motor binds to this cytoskeletal filament. Whether the motor strongly binds to the filament immediately upon first contact is not clear. Is the physical contact between motor and filament sufficient for binding, or are chemical processes needed as well? Due to the challenges in disentangling these steps, there is enormous variety in the reported ranges for binding rates. While landing rate assays [82] provide direct measurements of motor-cargo association rates, these do not inform motor-cytoskeletal rates. With the exception of [25], very little data of direct measurements of motor-microtubule binding events exists, but this study corresponds to the reattachment of a secondary motor that is kept close to the filament by another. Effective binding on the timescale of seconds [123, 27] to tenths of a second [60] have been reported from indirect measurements and utilized heavily in other modeling works [54, 50, 72, 71] to understand collective motor behavior. However, these effective rates neglect geometric factors (such as organization on the cargo) that are known to crucially dictate the binding rate [63, 93, 125, 11]. A mechanistic, biophysical model of the binding process is therefore necessary to reconcile the various experimental observations and modeling efforts.

Here, we use a combined experimental and computational approach to explore different possible biophysical models of how the motor-microtubule binding process occurs. The investigation is based on the initial association time between a cargo-bound kinesin and microtubule from recent optical trap measurements (Figure 2.1) on a variety of motor lengths

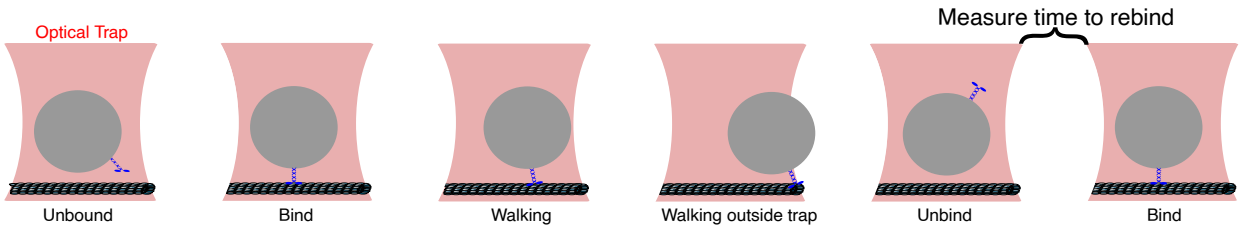

Figure 2.1: Experimental setup. An optical trap (pink) controls the average z-position of a polystyrene microbead cargo. When the cargo-motor ensemble binds to the microtubule and begins to walk on it, a position-sensitive diode (PSD) senses the displacement of the bead. As the motor walks farther from the center of the trap, the force on the cargo (and consequently the motor) grows, eventually leading to unbinding from the microtubule and resetting of the setup. The PSD measurements provide the timing between unbinding to rebinding, the binding process modeled throughout the remainder of the work.

and trapped distances away from the microtubule. The span of setups allows exploration and validation of models otherwise impossible with a single dataset. We first investigate the null model of a diffusion-limited search performed by the motor head. Through Brownian dynamics simulations coupled with simulation-based inference, we find that this model fails to capture a delay in binding at close distances. We find reconciliation with the data after the addition of an ADP-release requirement prior to binding to the model, motivated by known mechano-chemistry of motors. Through approximate Bayesian computation techniques, we quantify underlying rates and biophysical parameters governing this process and predict that most motor binding events are limited by tubulin-stimulated ADP release. Lastly, we provide predictions on how this process can be modulated distinctly by varying environmental concentrations or spatial distance, highlighting the complexity and regulatability of this interaction. Altogether, our study provides a new state-of-the-art mechanistic understanding of the motor-cytoskeletal binding process, a crucial ingredient in understanding the self-organization of motor-cytoskeletal assemblies used in cellular function. More broadly, our work illustrates how complexities arising from spatial and chemo-mechanical factors that shape protein-protein interactions may be understood through the combined efforts of theory and experiments.

2.3 Results

2.3.1 Diffusion-limited binding does not capture the qualitative behavior of experimental data

To investigate the biophysical mechanisms of the first association between a cargo-bound motor and a microtubule, we compare binding time data of three kinesin lengths (33, 45, and 60 nm) attached to a polystyrene bead that is laser-trapped at several distances away (0, 20, 40, and 60 nm) from a microtubule. Concentrations of motors in solution are diluted such that at most one motor is on each bead. Throughout the remainder of the work, we consider the binding time to be that between the unbinding reset event and the next time of detectable motion of the bead, as schematically shown in Figure 2.1. See Materials and Methods for further details on the experimental setup. The resulting binding times can be seen in Figure 2.2 ABC (black). Times are on the order of seconds, which is in line with other measurements of binding as discussed in the Introduction. Intuitively, as the cargo is moved away from the microtubule track, binding times increase. The most straightforward explanation for this is a "random search" mechanism rate-limiting the binding, schematically shown in Figure 2.3 as the "diffusion model". That is, the "null" model for binding, as assumed elsewhere [130], is that the motor head undergoes random motion until it reaches close proximity to the microtubule track and then binds with some reactivity. Our work does not directly incorporate electrostatic effects known to underlie the binding process [34], but assumes that these effects can be lumped into the effective reactivity and movement parameters.

To investigate whether such a diffusion-binding model can explain the binding time across experimentally observed conditions, we developed a Brownian dynamics simulation of the proposed model. The stochastic model includes the random motion of the cargo, both

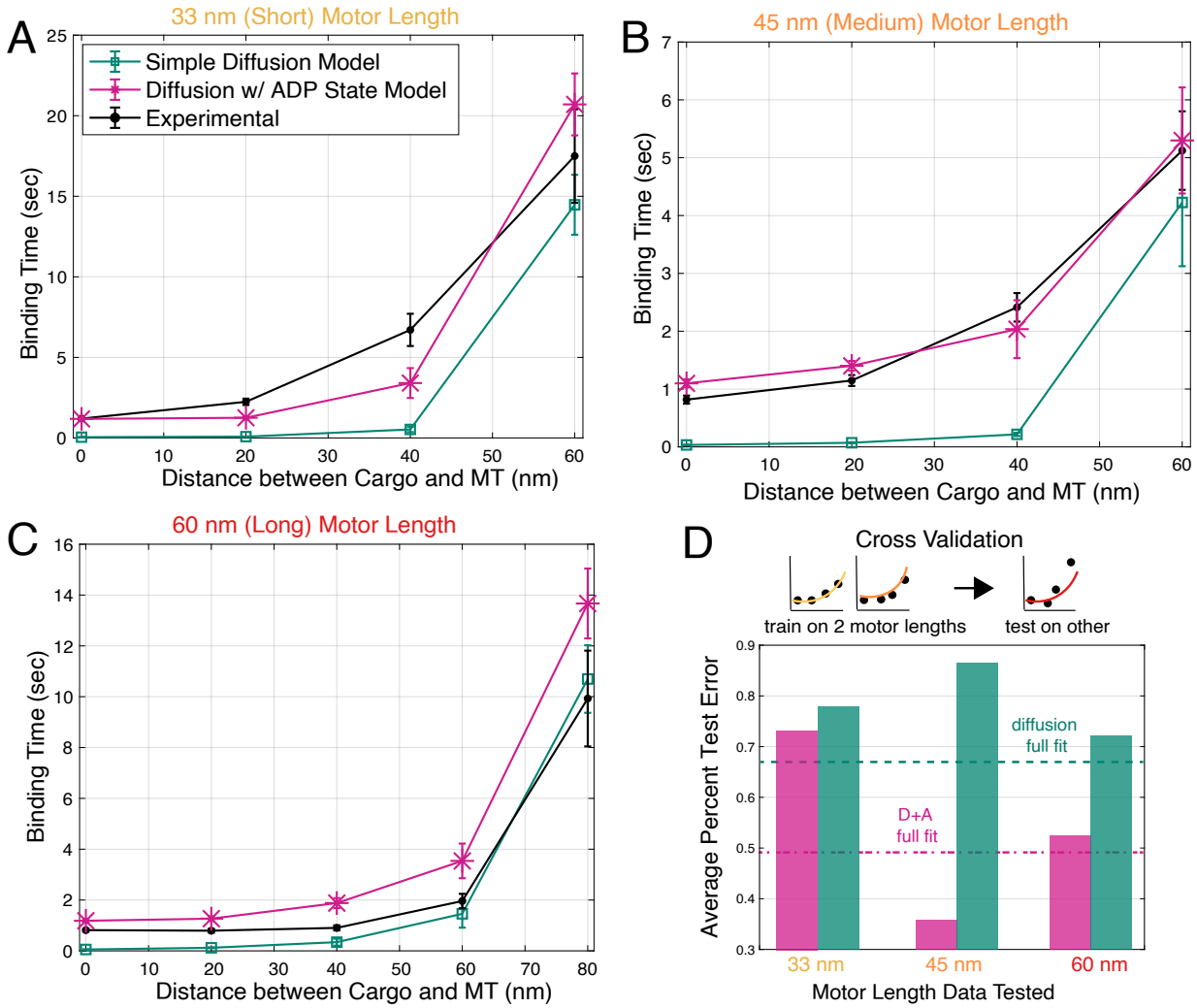

Figure 2.2: Model fits and cross-validation. ADP-release model captures qualitative behavior in experimental data, while the simple diffusion model cannot. *In vitro* optical trap experiments were used to measure mean binding times (black) for three motor lengths: 33 nm (A), 45 nm (B), and 60 nm (C). The horizontal axis shows average distances between the cargo and microtubule (MT), which were varied for each experiment. Two binding models (simple diffusion only in green and ADP-release in pink) were simulated and fitted to all of the experimental data. $n = 100$ for simulated data varied for experimental data. Data are presented as mean $\pm$ SEM. (D): Cross-validation was performed to determine the predictive power of each model. For three rounds, data was trained on two motor lengths, and tested on the third. Dashed lines show error when fitting the models to the entire data in ABC.

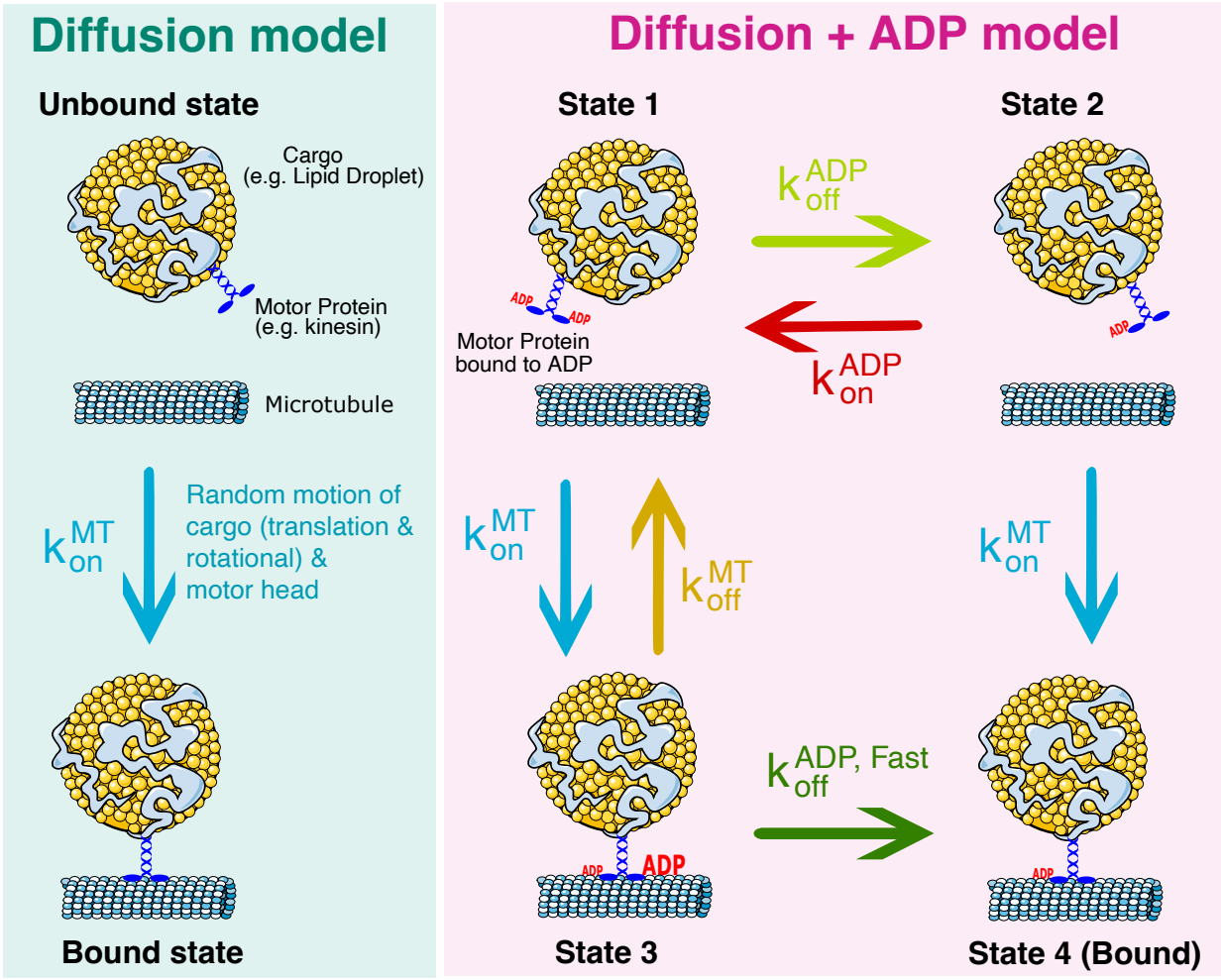

Figure 2.3: Schematic of models. Left: State diagram of the simple diffusion model of kinesin-microtubule binding. Through random motion of the cargo and motor head, binding time is determined by the stochastic search process of the motor reacting when in close proximity to the microtubule. Right: Model of binding process that considers a weak-to-strong transition driven by ADP release. We consider a cargo-motor ensemble that is in State 1, unbound from the microtubule and bound to ADP on both motor heads. From here, the motor can release ADP from one of its heads, transitioning to State 2, or bind weakly to the microtubule in State 3. To bind strongly to the microtubule and transition to State 4, the motor must meet two requirements: ADP is released from one of its motor heads and it must be within a binding distance to the microtubule. We consider two types of ADP release: a non-tubulin stimulated rate ($k_{\text{off}}^{\text{ADP}}$), and a faster tubulin-stimulated rate ($k_{\text{off}}^{\text{ADP,Fast}}$).

translation and rotational, and the diffusive search of a motor head attached via a tether to this cargo. The tether is assumed to be of the known length of each motor and exerts a Hookean force when extended beyond this length. The initial configuration of the motor head is assumed to be downward, based on the fast timescale of resetting in the optical trap (tenths of a second). When the motor head enters a specified distance of the microtubule due to random motion, the binding reaction occurs at an unknown, microscopic rate. Additional model details and discussion of assumptions can be found in the Materials and Methods. Ultimately, this leads to two unknown parameters: the diffusivity of the motor head, and the microscopic reactivity.

Through a suite of simulation-based inference techniques [1, 103, 120] (further details in Methods and Materials), we obtain fits to the diffusion model over all experimental setups for the two unknown parameters: the diffusivity of the motor head, and the microscopic binding rate. The resulting fits can be seen in Figure 2.2 ABC (green) for the mean time to bind for the three motor lengths and various distances. There appears to be reasonable qualitative agreement with the experiments, where increasing distances increases binding time. The corresponding parameter fits can be found in Table 2.1. While the diffusivity of the motor head is challenging to quantify [130], our fitted value on the order of 1000-10000 nm^2/s is within ranges considered for kinesin elsewhere [126]. Upon further scrutiny, the mean binding times shown in Figure 2.2 ABC, especially at close distances, display a distinct qualitative disagreement between the diffusion model and experimental measurements. In the diffusion model, as the cargo is trapped closer, the motor is effectively instantly able to bind. However, experimental values show a plateau of times around 1 second, even for close distances. This plateau points to the binding process being a multistep process.

Table 2.1: Fitted Parameters. D_{m} is the diffusion constant of the tethered motor head. κ_{w} is the stiffness constant of the weak bond between the motor and the microtubule when the motor is weakly bound to it. Parameters are fitted using a Bayesian optimization algorithm [1]. Some parameters were not found in previous literature.

Parameter	Simple Diffusion Model	Diffusion w/ ADP State Model	Previous Literature
$k_{\mathrm{off}}^{\mathrm{ADP}}$ (s^{-1})	0	0.008	0.008-0.1 [37, 26, 100, 101]
$k_{\mathrm{off}}^{\mathrm{ADP,fast}}$ (s^{-1})	0	2.12	0.5-300 [38, 26, 41, 100, 101, 105, 29, 2]
$k_{\mathrm{on}}^{\mathrm{ADP}}$ (s^{-1})	0	883.9	425.0 [26]
$k_{\mathrm{on}}^{\mathrm{MT}}$ (s^{-1})	80.6	70.65	
$k_{\mathrm{off}}^{\mathrm{MT}}$ (s^{-1})	0	0.2	0.31 [40]
D_{m} $(\mathrm{nm}^2\,\mathrm{s}^{-1})$	4459.8	1994.0	
κ_{w} $(\mathrm{pN\,nm}^{-1})$	0	0.0020	

2.3.2 A chemo-mechanical ADP-release model of binding better explains observed one second binding delay

With the observation that a simple diffusion model does not produce the ~ 1 second delay in binding at close distances seen in experimental measurements, we sought a model that may explain this phenomenon. Several plausible explanations including cargo rotation and measurement error were considered, but seem unlikely when evaluated with estimates of their effect (see Discussion). Instead, we turn to the rich mechanochemistry of the kinesin motor. It is known that the nucleotide state of each motor head crucially determines its strong or weak affinity to the microtubule [113, 19, 3] and through cycles of this nucleotide state (ATP, ADP, released), processive stepping is achieved [73]. We posit that this nucleotide-based regulation of "binding" extends beyond that of processive stepping, and even the preliminary attachment between the cargo-motor ensemble and the microtubule. That is,

we posit that the experimentally observed binding times correspond to a strong binding event, and therefore the underlying nucleotide state of the motor heads, plays a significant role in arriving at this state.

To investigate whether a model including nucleotide state may better explain the experimentally observed times, we extend the model to account for 4 possible states, as shown in Figure 2.3. In this model, the motor-cargo ensemble begins in State 1 with both motor heads in an ADP state, undergoing the same random motion as the diffusion model. From here, the ensemble can enter one of two states: State 2, where ADP is released from either motor head, or State 3, when the ensemble diffuses close to the microtubule and one of the motor heads weakly binds to it. From either of these states, the ensemble can then strongly bind to the microtubule either through diffusion (from State 2), or the ADP molecule is released (from State 3). We consider two types of ADP release, a fast tubulin-stimulated release and a slow non-tubulin-stimulated release [37, 100, 41, 38, 101, 26]. We consider ADP release as a requirement for strong binding based on the neck-linker model for stepping where an ADP-bound head has a low affinity for the microtubule, then this trailing head moves forward along the microtubule bound to ADP, and when it steps down onto the microtubule, ADP is released [131]. Importantly, our description is coarse-grained to not track the heads separately, but we consider the ADP release to describe either motor head. The assumption that the ensemble begins in State 1 has two parts: we assume that if the motor detaches in an ATP-bound state, this phosphate release is fast [73], but then the corresponding ADP release is slower without tubulin [38].

Using the same simulation-based inference approaches for the diffusion model, we fit the observed binding times for all 3 motor lengths and distances simultaneously for the extended ADP-diffusion model, with 7 unknown parameters, 2 from the diffusion model, 4 reaction rates, and 1 corresponding to the strength of attachment in the weak binding state. The result of the fits can be seen in Figure 2.2 ABC in pink. The overall fit is discernibly better

for the 33 nm and 45 nm motor lengths, and arguably worse for 60 nm at long distances. The noteworthy consistent overestimation for the 60 nm motor arises due to the simultaneous fitting of fixed parameters across all three motor lengths, sacrificing better fits for shorter motor lengths at the expense of the longest length. Such consistent overestimation does point toward a shortcoming of the model and may be due to heterogeneities in the different motors beyond their length alone. However, the model now captures the qualitative feature of a plateau of times at short distances. While only the mean binding times were used to fit, Figures A.2 and A.3 show close agreement in full distributions of binding times as well.

Beyond the qualitative improvement, the inherent danger in quantitatively assessing whether the ADP-release model better explains the data comes from the increased model complexity [13]. Intuitively, a model with more parameters has more flexibility to produce a better fit, and careful attention must be paid to model selection. In lieu of commonly-used information-theoretic techniques (AIC, BIC), even for simulation-based inference [65], we instead leverage the structure of our experimental observations to compare models based on their ability to explain unseen experimental circumstances. We perform a cross-validation procedure where we fit both the diffusion and ADP+diffusion models to the binding times for 2 of the 3 motor lengths, withholding one for testing on the trained models. In each validation test of withholding a motor length, the more complex model generalized better, shown in Figure 2.2D. From this, we conclude that the ADP-diffusion model better fits the observed binding times, even under cross-validation-based scrutiny [129].

2.3.3 Kinetic and biophysical parameters of the ADP-binding model can be estimated with high precision

Beyond the qualitative lesson of identifying the ADP-diffusion model as explaining the data, our fitting procedure provides rich quantitative insight into the underlying processes by es-

timating underlying parameters, shown in Table 2.1 and Figure 2.4. Some kinetic rates have been previously measured, and serve as support for the model, whereas others are, as far as we know, unmeasured. The values reported in Table 2.1 are point estimates from a simulation-based inference optimization procedure [1]. The estimated values for microscopic binding rate, diffusion of the motor head, and ADP binding are all within an order of magnitude of previously reported estimates, even after considering a smaller motor-microtubule binding radius (Figure A.11). To our knowledge, the weak-tethering strength κ_w has not been reported elsewhere, but we note it is significantly weaker than other physical forces in the system and may correspond to electrostatic attraction. The limiting ADP release rate estimated by our model is $\approx 2/\text{s}$. This parameter has a wide range of values reported in the literature, ranging from slow rates in the vicinity of ours, as well as significantly faster rates on the order of hundreds per second. We defer discussion of this important parameter and its subtle interpretation to the Discussion. As further validation of this optimization procedure for point estimates, we also performed a separate simulation-based inference technique, sequential approximate Bayesian computation (sABC) [103] to obtain samples of an (approximate) posterior distribution shown in Figure 2.4. The reason for this method was two-fold: for one, the agreement between the point estimates arising from the two procedures validates the approximations involved in the techniques, and the latter sABC approach produces valuable uncertainty quantification that we were unable to employ but may very well be possible using the techniques of [1]. Further details on these procedures can be found in the Materials and Methods. Somewhat surprisingly, all parameters of the model seem to be identifiable, as shown in the relatively tightly-shaped posterior distributions.

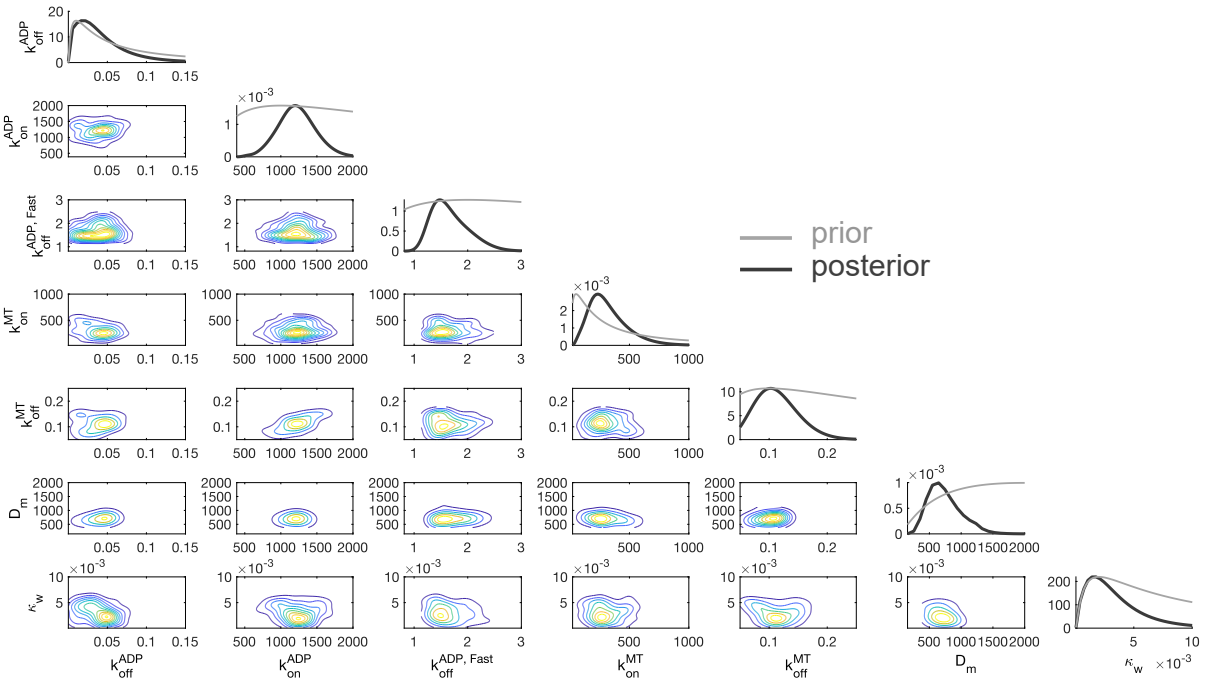

Figure 2.4: Estimates of microscopic parameters from fitting the ADP-diffusion model. Joint (Approximate) Posterior Distribution of ADP release Model Parameters. Black curves in the marginal densities from sequential approximate Bayesian Computation (sABC) are the posterior distributions, and the grey curves are the priors. A kernel density estimator [43] was applied to discrete samples to form posterior estimate curves.

2.3.4 Most motors strongly bind via tubulin-stimulated ADP release

These quantitative estimates of the underlying microscopic rates provide qualitative lessons about motor binding. Referring to the model schematic in Figure 2.3, motors can achieve the strong binding state either through an intermediate weak binding state (State 3) after which ADP release occurs, or directly from a diffusing state (State 2). Although we do not observe these transitions directly, their relative proportions can be deduced from the data and are investigated in Figure 2.5. Our proposed binding process can be conceptually decomposed into two components: the physical search process of the motor binding (either weakly or strongly) to the microtubule, and an ADP release step. Figure 2.5A demonstrates the predicted relative contribution of the physical search component to the overall binding time. Specifically, the panel shows the fraction of time stochastic simulations of the full binding process spent in States 1 and 2, where the motor is unbound completely and searching for the microtubule. This fraction was calculated by determining the portions of time spend unbound in each simulation, and then taking the average. For all motor lengths, the fraction of time in the searching state increases as the distance between the cargo and microtubule increases, ranging from about 20% to 80% of full binding time. Moreover, for a fixed distance (60 nm), the fraction of time searching increases as the length of the motor decreases. These trends can be interpreted as the diffusion-based physical search step always contributing a meaningful rate limitation to the process. However, from this panel alone, the typical binding pathway cannot be deduced. As physical search takes varying of the portion of the total binding time, is ADP release always, never, or sometimes the rate-limiting component? Figure 2.5B addresses this question by computing the fraction of stochastic simulations that end up strongly bound (State 4) by entering through the tubulin-stimulated ADP release pathway (from State 3). These portions show that for all motor lengths and distances, effectively all binding events (about 99%) enter through this state.

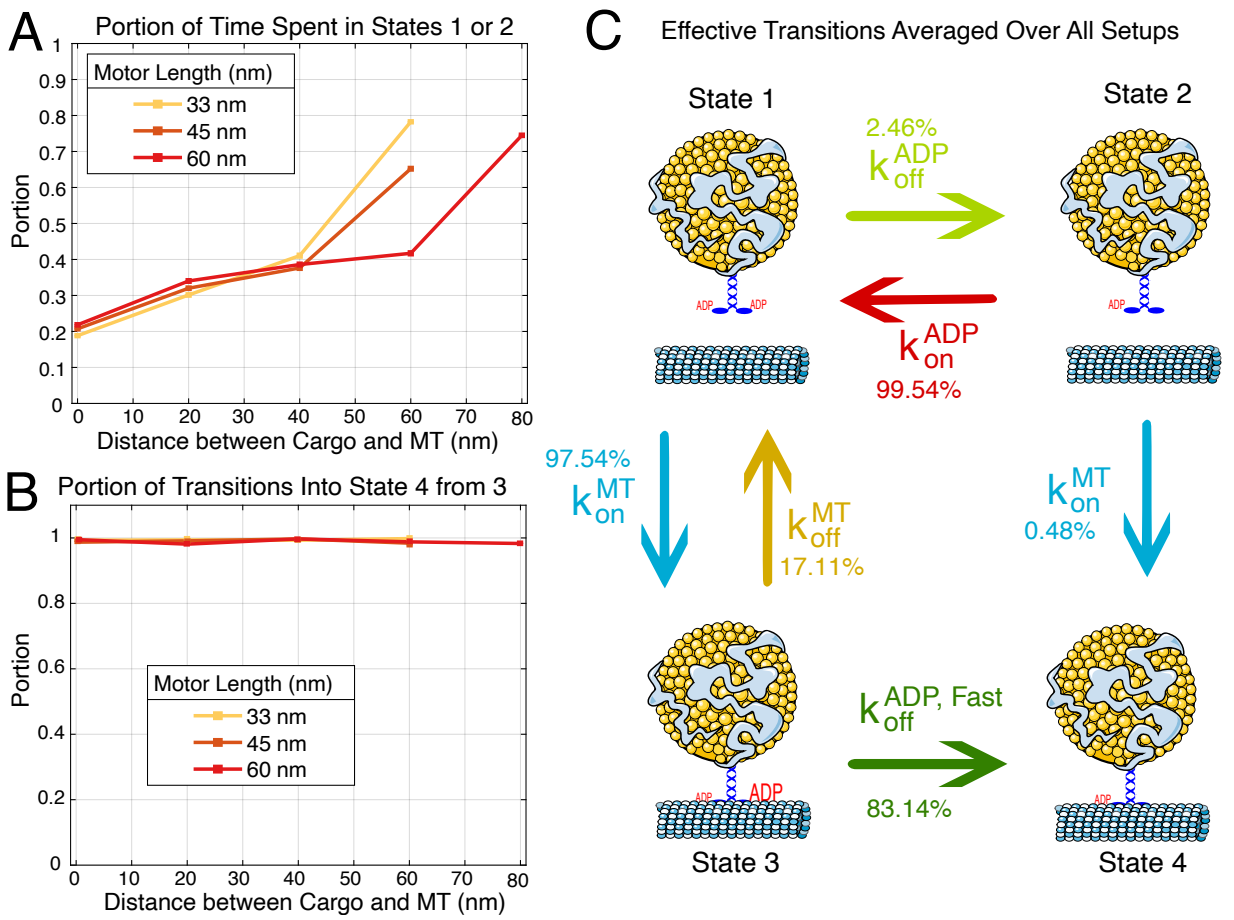

Figure 2.5: Cataloging pathways of binding from stochastic simulation shows that motors typically bind via tubulin-stimulated ADP release. Panel A: Portion of total binding time (into state 4) spent in the unbound states (1 and 2) for all motor lengths and distances. this portion increases. Panel B: Portion of all binding events that weakly and then strongly bind (arrive in state 4 from state 3) from state 3 (as opposed to arriving from state 2). Panel C: Mean percent of transitions that occur from each state, averaged over all events from all experimental conditions (motor length and mean spacing between cargo and microtubule). Parameters for simulation are from Table 2.1.

Motors could, in theory, release ADP while undergoing diffusive search, and then strongly bind directly (States 2 to 4). To understand why this pathway does not seem to contribute to the binding time, we show the full effective predicted binding transition frequencies in 2.5C, averaged over all motor lengths and distances. A full report of the relative proportions and effective rates of each transition can be found in Figures A.4 and A.5. From State 1, most (over 80%) of initial binding interactions arise via a preliminary weak binding state and subsequent ADP release (States 3 to 4). However, we predict that some transitions to State 2 (ADP release while unbound) occur. From State 2, there may seem to be a paradox that the transition rate between States 2 to 4 is very low, which one might interpret as the ADP released motor state having *low* affinity for the microtubule, but we emphasize this quantity is a byproduct of the competing rates between physical binding and ADP capture. That is, State 2 does not have a lower affinity for the microtubule, but rather, occurs less often than ADP rebinding. Therefore, the ADP release before physical search is too transient to provide a viable binding pathway. Altogether, our results suggest tubulin-stimulated ADP-release after weak binding is the typical pathway for kinesin binding.

2.3.5 Binding rates can be distinctly modified by physical and chemical factors

The quantity and structure of experimental data have thus far allowed for significant progress in understanding binding from retrodictive reconciliation with a model. We conclude with predictions that emphasize the broader lessons and may serve as the basis of validation in future experiments. The exploration of typical binding events in the previous section points toward conceptualizing this process as a distinct mechanical diffusive search and a chemical step from the nucleotide state. Regulation and perturbations of each of these components should therefore be discernible. To explore these two scenarios, we predict how the binding times should be altered in two hypothetical experimental perturbations shown in Figure 2.6.

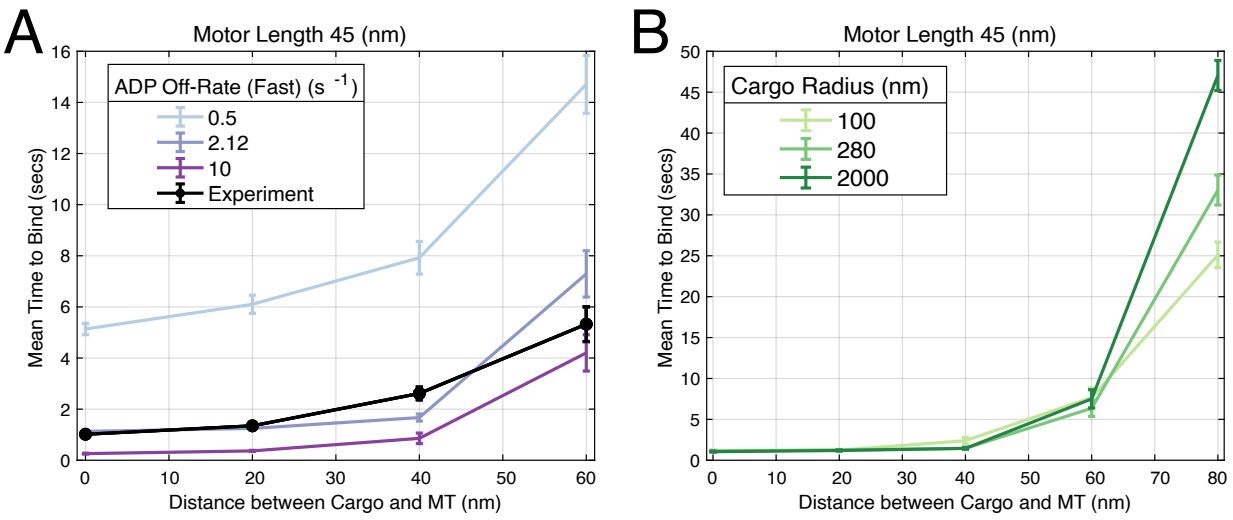

Figure 2.6: Predicted binding time changes from chemical and physical perturbations. A: An example of a chemical change, $k_{\text{off}}^{\text{ADP,Fast}}$, was varied in the simulation and resulting simulated binding times are plotted. Data are presented as mean ± SEM. B: Physical changes, such as changing the cargo size, can also be made to study the resulting binding times.

In the first, panel A shows how if one could modulate the tubulin-stimulated ADP-release rate, the effective spatially-dependent binding rate shifts up or downward for all distances. In contrast, numerous physical experiments could plausibly alter the physical properties of the system. In Figure 2.6B, we show the predicted effect of changing the cargo size, which would consequently modify the overall diffusivity of the ensemble and the random search time. For short distances that are not limited by this diffusive search, the difference is negligible, but for long distances, the effect becomes magnified. Predictions for other motor lengths can be found in Figure A.6. While we do not currently have the technological capability to validate these experimental predictions (e.g., the ability to disentangle the competition between ADP and ATP binding to the motor head prior to the motor binding), we hope they will be the basis of future validation or invalidation of our proposed binding model.

2.4 Discussion

2.4.1 Conclusion

Altogether, our results point toward a model of the initial binding between a cargo-bound kinesin and a microtubule track being more complex than a diffusion-limited search of the motor head that is presumed elsewhere [130, 126]. Motivated by the known mechano-chemistry of motor stepping, where the nucleotide state of each motor head dictates microtubule affinity [9, 37, 38], we posit that the observed binding times correspond to a nucleotide-state-limited strong binding event. In this conceptual model, the primary binding pathway is a preliminary weak binding from physical search, followed by the motor being weakly tethered to the microtubule. During this weak tethering, ADP is released from one of the heads and the motor becomes strongly bound. The rate-limiting component transitions between ADP release and physical search as the cargo-microtubule distance increases, arising from the competition between these rates. To validate this hypothesis, we considered a coarse-grained computational model that incorporates both diffusive search and the ADP state of motor heads, and through simulation-based inference and model selection, ultimately found compelling agreement with the experimental measurements. With only observed binding times, computational modeling reveals unobserved details of the binding process and predicts that the "typical" binding event is modulated distinctly by both environmental and physical factors. From a design perspective, these orthogonal modulations allow for more fine-grained control and malleability than either separately.

The emergent model of an ADP-release rate-limiting kinesin binding warrants further discussion. Due to the inability to observe the behavior of individual motor heads, our computational model forgoes this complexity and implements weak and strong binding states agnostic to the underlying biochemistry. The simulation-based inference procedure and its validation rigorously show that a model with this weak-to-strong transition fits the binding

data more closely than without these states. This agreement primarily arises from the fitted ≈2/s rate of strong binding after weak binding. Based on the known mechanochemistry of kinesin, we attribute this weak-to-strong transition to an ADP release of one of the motor heads [9, 37, 38]. However, this rate is commonly reported on the order of ≈100/s [29], allowing for the rapid procession of the motor on this same rate-limiting timescale. This presents an apparent contradiction to our hypothesis, as this fast rate indeed fails to explain the apparent delay seen in binding times. Reconciliation arises from the findings of [105], principally the result that ADP release rate of each kinesin head is highly sensitive to the load applied to it. When both kinesin heads are bound to the microtubule, the release rate for ADP from the front head (under load) is indeed very rapid. However, The ADP release rate for kinesin when only a single head is bound (and not under load) is much lower. Our model describes the transition from kinesin completely unbound to the MT to a single-head attachment and therefore corresponds to this slow unloaded, microtubule-stimulated ADP release rate. This slower ADP release rate has been reported in the literature with noteworthy agreement with our estimated rate. In [28], the authors find a bimodal distribution of ADP release rates: one fast, and a second, slower rate of 0.4-2.3/s. This is in close agreement with the rates of 2.3-3.3/s found in [100]. These same authors later report a faster value of 31.5/s [101], but note this is an average of fast and slow rates. In a more recent study [2] find an ADP exchange rate of ≈0.5/s that can be modulated by engineering longer neck linkers. Indeed, like these studies, our work cannot resolve the precise underlying biochemistry of individual motor heads. However, the remarkable agreement between the fitted weak-to-strong transition rate arising from our work and the slow unloaded ADP release found in the literature provides convincing evidence of their connection. Moreover, the emergence of the unloaded ADP rate reveals more insight into the underlying mechanics between the motor heads in the attachment process.

Motor binding times have been estimated and measured many times prior [123, 27, 82, 25], but these studies cannot easily disentangle the physical configuration the binding arises

from, whether it be from a landing experiment, DNA origami, or motors re-attaching while another is already bound. The absence of this consideration juxtaposes the increasing body of evidence that spatial organization plays a vital role in motor binding [63, 93, 125, 11]. By distilling both the experimental assay and corresponding model to the minimal ingredients of a single motor attachment, we can clarify this process with unprecedented precision and generalizability. That is, while we have shown that our model successfully recapitulates the experimental data from our optical trap assay, we have moreover provided quantitative details about the underlying process that can be used to calculate binding times in other configurations. That is, one could imagine taking our fitted model and adapting it to DNA-origami cargo to reconcile the observed binding rates of [27, 25]. Discrepancies between the predictions and observations may occur, but these provide crucial details about the underlying chemistry and physics that we advocate warrant further investigation.

2.4.2 Limitations and Assumptions

We have not, and likely cannot ever fully rule out other conceptual models and confounding factors of binding time. The key qualitative feature we sought to replicate was the binding delay on the order of 1 second in close-proximity cargoes. Our ADP release model successfully recapitulates this, and we provide testable hypotheses that can be used to invalidate the model in Figure 2.6. We considered several other possible factors that may explain or contribute to this delay. The most pressing possibility is whether this delay arises as an artifact of failure to detect optical trap displacements faster than this. Assuming an unloaded kinesin velocity of around 500 to 1000 nm/s, a 15 nm bead displacement for detection corresponds to fractions of a second and does not explain the observed delay on the order of a second. Furthermore, we struggle to speculate what a realistic initial configuration of the motor may be, as a more detailed model of the cargo resetting in the optical trap likely requires consideration of hydrodynamic effects that couple rotation, motion, and distant-

dependent diffusivity [106]. We made the crude assumption that the motor was configured downward initially due to the fast timescale between cargo resetting in the trap, but this is likely not the case. However, based on our estimates (Figure A.7) and others estimate [11] a cargo taking 0.2 seconds to complete a full rotation at this viscosity. To test the robustness of this result, we extended the model to also approximately incorporate near-wall diffusivity hindrance from hydrodynamics [31, 15, 59] and find that there is some slowdown at far distances with random initial motor configurations, shown in Figure A.10. In a previous study from the lab [12], it was found that a reduced bead size does reduce the binding time slightly. Altogether this evidence points toward supporting our conceptual model that cargo rotation and hydrodynamics do play a role in motor binding time, but alone fail to explain the magnitude of delay seen at close binding distances. One last possibility we note is the conceptual model where a motor begins in a "crumpled" state, and then unfurls with some delay to bind. Our model of the kinesin stalk is crude, and one could imagine other possibilities such as a worm-like chain model considered for the neck linker [55]. However, these models primarily differ when under load, rather than undergoing a diffusive search. Therefore, we leave the investigation of other polymer models for the stalk to future work. We note the coarse-grained approximation of the whole motor head as a single spatial point with a single nucleotide state due to the inability to resolve further detail from available data. We leave to future work more detailed models that incorporate *in vivo* complexities, including motor attachments diffusing on the surface of cargo [63, 93, 125] or cargoes with with multiple motors. Lastly, we identify that this binding model may be limited to kinesin, and perhaps even only some kinesins. Future investigation warrants investigating other motors binding details, e.g., dynein, through the procedure outlined in this work. When more details, such as the dynein on- and off-rates, can be brought to light, these details can be combined with our work to understand our model's and the observed binding delay's context *in vivo*.

2.4.3 Context in Cytoskeletal-Motor Systems

The focus of this work is understanding the binding between a single cargo-bound kinesin and a microtubule track. This setup follows the spirit of a now long-established and successful line of investigation of cytoskeletal-motor assemblies by isolating fundamental building blocks. We attempt to situate our advances in the broader context of the wildly complex array of cytoskeletal-motor interactions and the feedback between them. We emphasize the chemo-mechanical nature of our binding model in the context of the enormous literature on how physical and chemical changes to microtubules affect motor behavior. For instance, geometry of the microtubule network dictates cargo-microtubule distances [17, 74] by pulling the cargo closer to the microtubule via tethers such as dynactin [4], or pushing it away via microtubule-associating proteins (MAPs) [56], and motors themselves reorganize microtubules through forces [126]. A zoo of microtubule-associating-proteins (MAPs) and the tubulin code are known to interfere with motor function [46, 102], including in the recruitment of motors [45, 61, 23]. Our model may shed light on explaining the mechanisms by which these microtubule decorations modify motor binding, and serve as the basis for future investigation. Through the decomposition of how chemical and physical factors modulate binding, our study may be the basis for discerning the mechanism of MAPs regulation of motors. For instance, one could imagine C-terminal tails may serve as physical tethers or may alter nucleotide states, and such an investigation remains for the future. More broadly, this understanding serves as a key step toward understanding how cells regulate binding to direct cargo and perform even more cytoskeletal-motor functions such as coordinate mitosis [81]. Moreover, this understanding may help aid in the design of increasingly sophisticated synthetic systems [92], where spatial distances can be prescribed.

2.4.4 Broader Lessons for Probing Protein-Protein Interactions

The difficulty in directly observing protein-protein interactions makes their study challenging. Two main avenues of approaches have been historically successful, each at extremes of chosen level of detail. Molecular dynamics simulations are a gold standard for predicting interactions. We build on the immense insight they have illuminated on the interactions between microtubules and kinesin [83, 99] and otherwise would not have considered the ADP release in our model. However, these approaches built from microscopic components have immense difficulty in scaling up to more complex systems with multiple interacting components, such as between motor, cargo, and cytoskeletal filaments. At the other extreme, "spherical cow" models of diffusion-limited reactions [107, 42] have revealed many qualitative lessons of protein-protein interactions, but remain challenging to quantitatively link with data because even the inclusion of modest complexities like orientation constraints [8] make the analyses prohibitively complex.

Our work adds a timely vignette to other studies [6, 132, 32] that illustrates the value of striking an intermediate level of complexity in understanding protein-protein interactions. This balance allows for the incorporation of microscopic details from more fine-grained studies but remains vigilantly coarse-grained to directly connect with data. We highlight major components of the work that we believe will be of broader use in other probing of protein-protein interactions, such as understanding the competition between peptides and kinases for the same binding site on a transcription factor, or disentangling folding and aggregration rates in protein. For one, we leveraged measuring interactions in a variety of conditions. Equipped with only a single motor length or trapped distance, the diffusion model would have fit to a seemingly satisfactory degree. By probing a model's ability to explain data across conditions, we were able to identify the ADP model. Furthermore, our work was made possible by recent advances in simulation-based inference [18]. While model fitting has historically been bogged down in the complications of the procedure, we now live in an

age where it is plausible to perform inference on any model that can be thought of (and simulated), with rapidly improving techniques beyond those we utilized in this work [66]. Neither of these lessons is specific to the context of cytoskeletal-motor interactions, and therefore we hope serves as an outline for other pursuits in data-driven discovery of protein-protein interactions.

2.5 Methods

2.5.1 Optical Trap Experiments

The optical trapping setup was assembled on an inverted Nikon TE200 microscope using a 980 nm, single mode, fiber-coupled diode laser (EM4 Inc). The laser power was set to achieve a trap stiffness, κ_t, of $\sim$0.045 pN nm^{-1} while using the polystyrene bead of 0.56 μm (streptavidin conjugated, Spherotech).

Single motor experiments were carried out in the motility buffer (80 mM Pipes pH 6.9, 50 mM CH3COOK, 4 mM MgSO4, 1 mM DTT, 1 mm EGTA, 10 μM taxol, 1 mg mL^{-1} casein). In all the rebinding rate assays, single-motor kinesin-coated polystyrene beads were prepared just before the measurements. The motors DK-406-His/DK-560-His/DK-746-His (Kinesin-1, aa 1-560/Drosophila Kinesin aa 1-406/ Drosophila Kinesin aa 1-746; His tag at c-term) were diluted to $\sim$20 nM before mixing with $\sim$1 pM of biotinylated penta-His- antibody conjugated streptavidin beads stored at 4°C. This ratio produced the bead binding fraction of 10-15% and was maintained to maximize the probability of finding single motor beads in the solution (a bead binding fraction less than 30% corresponds to a single motor regime [10]). The bead-motor incubation ($\sim$50 μL volume) was carried out at room temperature for 10 minutes. At the end of incubation, the sample chamber with preassembled microtubules was washed with $\sim$50 μL of warm filtered buffer just before injecting the incubated mixture.

Experiments were carried out at room temperature in a motility buffer supplemented with 2 mM ATP and oxygen-scavenging system (0.25 mg mL^{-1} glucose oxidase, 30 μg mL^{-1} catalase, 4.5 mg mL^{-1} glucose).

In general, small dust or debris in the solution gets pulled into the trap along with the bead. Trapped dust interferes with motor rebinding to microtubules. To prevent this interference, the large dust particles and aggregates of casein in the buffer were removed using a 100 nm centrifugal filter (Millipore). Another potential issue is the stage drift during measurement, and it was minimized with an automated drift correction system using an xyz piezo stage (PI) and custom software.

All kinesin proteins were purified using HIS-tag and MT affinity purification after expressing them in Rosetta bacterial cells as described earlier [89]. DK406 plasmid was procured from Addgene (plasmid ID #129764, generously supplied by William Hancock lab). DK746 was designed in the lab after modifying the full-length DK980, also procured from Addgene (plasmid ID: #129762, William Hancock lab), using restriction enzyme digestion.

2.5.1.1 Binding Detection

Bead displacements in the trap registered by a position-sensitive diode (PSD; First Sensor AG) were acquired at 3kHz using an analog-to-digital converter (ADC) card. The digitized PSD data was smoothed with a 40 point fast Fourier transform (FFT) filter and analyzed by custom Matlab code to score all the peaks greater than 15 nm and lasting more than 0.01 seconds (30 data points). The experimental method is fully described in [88].

2.5.1.2 Maintaining Bead-Microtubule Separation

Autocorrelated template matching of defocused fiduciary bead immobilized on the surface served as feedback signal to maintain a stable bead-microtubule separation. The method was developed using an autocorrelation of a template image with real-time images of the fiduciary beads to generate a parameter called match score (degree of matching). It is custom-developed to study protein-protein interactions using an optical trap. To describe it briefly, fiduciary beads were immobilized on the coverslip and an image of the bead was recorded at 200 nm below the surface to serve as a reference library image. The key parameter here is the match score (value = 0 for no match and 1000 for perfect match with the library image) and when the template used is a bead in focus, this score exhibits quadratic behavior in the vicinity of the surface. Thus, score change per nm of the focus shift is negligible when the bead is in perfect focus. However, when a defocused bead image is used as a reference library image, the score change/nm is as high as 1% for every 10 nm z-focus change. This parameter was used as a feedback signal both to increment and lock the z-position at a fixed level using an automated focus locking system developed in-house using an xyz-piezo-stage, image grabber cards, and labVIEW. In the experiments, the distance between the trapped bead and the Surface-attached microtubule is altered by moving the surface. In principle, moving the surface by causes a slightly smaller change (≈12% less) in the distance between the trapped bead and the surface, due to the mismatch in refractive indices. This has not been corrected for in the data presented.

2.5.2 Brownian Dynamics Simulation

The simulation consists of a motor that is bound to a cargo and a microtubule. The cargo is a three-dimensional sphere and is subject to translational and rotational diffusion. The motor's condition is dependent on whether an ADP molecule is bound to it and whether

it is bound to the microtubule. Whether the motor is weakly or strongly bound to the microtubule is dependent on whether it is bound to an ADP molecule. The transitions through these states (Figure 2.3) are simulated using a Gillespie-style algorithm [30]. The motor is defined by its location of attachment to the cargo and its head location. Locations of the motor head and cargo center are calculated using the Euler-Maruyama method [49]. The microscopic binding between the motor head and microtubule follows a standard "Doi model" for chemical reactions [68]: when the motor heads come within binding reach of the microtubule, it has a constant rate of binding to it; otherwise, this rate is 0. The motor behaves as a spring, and when they are bound, they experience and exert force. When the motor is weakly bound to the microtubule, its off-rate depends on force. ADP molecules can also bind and unbind to the motor head at constant rates, but the ADP off-rate is dependent on whether the motor is weakly bound to the microtubule. The equations of motion for the cargo and motor are constructed by discretizing a set of stochastic ordinary differential equations derived from force balance.

2.5.2.1 ADP Release Model Description

This model is three-dimensional and mesoscale. A set of stochastic ordinary differential equations is used to describe the location of the cargo sphere and the motor that is attached to it. The motor transitions stochastically between discrete states (Figure 2.3), and these transitions occur as Poisson processes. The force that the motor exerts on the cargo is modeled as a one-way spring:

$$\vec{F}^m\left(\vec{a},\vec{h}\right)=\begin{cases}-\kappa^m\left(\left|\vec{h}-\vec{a}\right|-L_m\right)\left(\frac{\vec{h}-\vec{a}}{\left|\vec{h}-\vec{a}\right|}\right)+\vec{F}^w & \left|\vec{h}-\vec{a}\right|>L_m\\ 0 & \left|\vec{h}-\vec{a}\right|\leq L_m\end{cases},$$

where $\vec{a}$ and $\vec{h}$ are the motor anchor and head locations, respectively, κ^m is the motor stiffness constant, L_m is the motor rest length,

$$\vec{F}^w = \begin{cases} \kappa^w \left(\vec{a}_{MT} - \vec{h} \right) & \text{motor is weakly bound to the MT} \\ 0 & \text{motor is unbound from the MT} \end{cases},$$

κ^w is the weak spring between the motor head and the microtubule, and $\vec{a}_{MT}$ is where the motor head is weakly bound on the microtubule. There is a torque that is exerted on the cargo:

$$\vec{\tau}^m \left(\vec{a}, \vec{h}, \vec{c} \right) = \begin{cases} (\vec{a} - \vec{c}) \times \vec{F}^m \left(\vec{a}, \vec{h} \right) & \text{weakly bound to MT} \\ 0 & \text{otherwise} \end{cases},$$

where $\vec{c}$ is the cargo center location. Thus, we have ordinary differential equations (modeled after the Langevin equation):

$$\frac{\mathrm{d}\tilde{\mathrm{c}}\,(\mathrm{t})}{\mathrm{dt}} = \frac{1}{6\pi\eta R}\vec{F}^m \left(\vec{a}\,(t)\,, \vec{h}\,(t) \right) + \frac{1}{6\pi\eta R}\vec{F}^b\,(t)\,, \tag{2.1}$$

and

$$\frac{\mathrm{d}\tilde{\theta}\,(\mathrm{t})}{\mathrm{dt}} = \frac{1}{8\pi\eta R^3}\vec{\tau}^m \left(\vec{a}\,(t)\,, \vec{h}\,(t)\,, \vec{c}\,(t) \right) + \frac{1}{8\pi\eta R^3}\vec{\tau}^b\,(t)\,, \tag{2.2}$$

where η is the water viscosity, R is the cargo sphere radius, θ is the cargo orientation, and $\vec{F}^b$ and $\vec{\tau}^b$ are the Brownian force and torque, respectively, which are random variables with mean 0 and variance $2k_BT\xi_c$, and ξ_c is the drag coefficient of the cargo. According to the

Euler-Maruyama method, a discrete formulation of Equations 2.1 and 2.2 will be:

$$\vec{c}\left(t_{n+1}\right) = \vec{c}\left(t_n\right) + \frac{1}{6\pi\eta R}\vec{F}^m\left(\vec{a}\left(t_n\right), \vec{h}\left(t_n\right)\right)\triangle t + \sqrt{2\frac{k_B T}{6\pi\eta R}\triangle t}\vec{G}_c\left(t_n\right)$$

and

$$\vec{\theta}\left(t_{n+1}\right) = \vec{\theta}\left(t_n\right) + \frac{1}{8\pi\eta R^3}\vec{\tau}^m\left(\vec{a}\left(t_n\right), \vec{h}\left(t_n\right), \vec{c}(t_n)\right)\triangle t + \sqrt{2\frac{k_B T}{8\pi\eta R^3}\triangle t}\vec{G}_\theta\left(t_n\right),$$

where n is the current time step, and $\vec{G}_c$ and $\vec{G}_\theta$ are mutually uncorrelated vectors of independent and identically distributed (i.i.d.) Gaussian random variables with mean 0 and variance 1. The cargo cannot phase through the microtubule. Since we are simulating optical trap experiments, we add a force from the trap on the cargo:

$$\vec{c}\left(t_{n+1}\right) = \vec{c}\left(t_n\right) + \kappa_t\left(\vec{c}(1) - \vec{c}\left(t_n\right)\right) \tag{2.3}$$

$$+ \frac{1}{6\pi\eta R}\vec{F}^m\left(\vec{a}\left(t_n\right), \vec{h}\left(t_n\right)\right)\triangle t + \sqrt{2\frac{k_B T}{6\pi\eta R}\triangle t}\vec{G}_c\left(t_n\right), \tag{2.4}$$

where κ_t is the trap stiffness. We can now determine the motor anchor location by inputting the cargo axis of rotation $\vec{\theta}\left(t_{n+1}\right) - \vec{\theta}\left(t_n\right)$ and this axis' length as the magnitude of rotation (in radians) into a rotation matrix $\mathbf{M}\left(t_n\right)$:

$$\vec{a}\left(t_{n+1}\right) = \mathbf{M}\left(t_n\right)\left(\vec{a}\left(t_n\right) - \vec{c}\left(t_n\right)\right) + \vec{c}\left(t_n\right) + \left(\vec{c}\left(t_{n+1}\right) - \vec{c}\left(t_n\right)\right). \tag{2.5}$$

Similarly to Equations 2.1 and 2.2, we discretize ordinary differential equations for the motor head position:

$$\vec{h}\left(t_{n+1}\right) = \vec{h}\left(t_n\right) + \frac{1}{\xi_m}\vec{F}^m \triangle t + \sqrt{2D_m}\vec{G}_m, \tag{2.6}$$

where $\xi_m = k_B T / D_m$ is the motor drag coefficient, D_m is the motor head diffusion constant, and $\vec{G}_m$ is the uncorrelated i.i.d. Gaussian random variable of mean 0 and variance 1. The motor head cannot phase through the microtubule and the cargo. Since in experiments, the microtubule lies on the coverslip surface, the motor head cannot diffuse under the microtubule. A list of all variables used are described in Table 2.2.

Table 2.2: **List of Variables.**

Variable	Description
$\vec{F}^m$	Force from motor head
$\vec{a}$	Position on cargo where motor is anchored
$\vec{h}$	Position of motor head
$\vec{F}^w$	Force from weak bond between the motor and the microtubule
$\vec{a}_{\mathrm{MT}}$	Position on microtubule where motor is weakly bound
$\vec{\tau}^m$	Torque that motor exerts on cargo
$\vec{c}$	Position of cargo center
$\vec{\theta}$	Cargo rotation
t_n	Time at the nth time step
$\vec{F}^b$	Brownian force
$\vec{\tau}^b$	Brownian torque
$\vec{G}_c$, $\vec{G}_\theta$ and $\vec{G}_m$	Gaussian random variables

We also considered an extended model that approximately accounts for the near-wall diffusivity hindrance from hydrodynamics [31, 15]. In lieu of fully incorporating the detailed

hydrodynamics, an undertaking outside the scope of this work [106, 85], we employ the classical Brenner correction formulae [31, 59]. As an approximation based on the assumption that the z-direction motion dominates the binding time, we rescale the entire rotational and translation drag coefficients of the cargo by the analytical perpendicular z-dependent rotational and translational diffusivities. Specifically, we rescale η in the translational update eqn. (2.4) by $(1-(9/8)(R/z)+(1/8)(R/z)^3)^{-1}$ and the translational η in eqn. (**??**) by $(1-(5/16)(R/z)^3+(15/256)(R/z)^6)^{-1}$ where R is the radius of the cargo and z is the distance from the cover slip to the center of the cargo. Notably, this neglects the asymmetry in perpendicular and parallel directions, and leave these details to future work.

Transitions between each motor state (Figure 2.3) are modeled as Poisson processes, with rates as follows:

$$\lambda_{\text{off}}^{\text{ADP}} = \begin{cases} k_{\text{off}}^{\text{ADP}} & \text{ADP-bound and MT-unbound} \\ k_{\text{off}}^{\text{ADP,Fast}} & \text{ADP-bound and weakly bound to MT} \\ 0 & \text{motor is ADP-unbound} \end{cases} \tag{2.7}$$

$$\lambda_{\text{on}}^{\text{ADP}} = \begin{cases} k_{\text{on}}^{\text{ADP}} & \text{motor is ADP-unbound} \\ 0 & \text{motor is ADP-bound} \end{cases} \tag{2.8}$$

$$\lambda_{\text{on}}^{\text{MT}} = \begin{cases} k_{\text{on}}^{\text{MT}} & \text{unbound from MT and within } d_{\text{MT}} \\ k_{\text{off}}^{\text{ADP,Fast}} & \text{motor is weakly bound to microtubule} \\ 0 & \text{motor is not within } d_{\text{MT}} \end{cases}, \tag{2.9}$$

where d_{MT} is the binding distance between the motor head and the microtubule, and

$$\lambda_{\mathrm{off}}^{\mathrm{MT}} = \begin{cases} k_{\mathrm{off}}^{\mathrm{MT}} \cdot \exp F^w/F^d & \text{weakly bound to MT} \\ 0 & \text{motor is MT-unbound} \end{cases}, \tag{2.10}$$

where F^d is the motor's critical detachment force. Parameter values are listed in Tables 2.1 and 2.3. The particular choice of $d_{\mathrm{MT}} = 5$nm was made based on the approximate size of kinesin-1, but varying this parameter has little effect on the resulting fit (cumulative absolute fitting errors were at most 0.01s different), shown in Figure A.11.

Table 2.3: Measured parameters. *Unmeasured estimate. †Measured estimate. The motor length includes the antibody that binds the motor to the cargo (about 10 nm).

Parameter	Description	Value
κ^m	Motor stiffness (pN/nm) [51]	0.3200
κ_t	Trap stiffness (pN/nm)†	[0.045 0.045 0.03]
L_m	Motor length (nm)†	Varies
η	Fluid Viscosity ($\mathrm{pN \cdot s/nm^2}$)	1e-05
R	Radius of cargo bead (nm)	280
k_bT	Boltmann constant ($\mathrm{pN \cdot nm}$)	4.114
d_{MT}	MT Binding range (nm)*	5
F^d	Critical detachment force (pN) [54]	4

2.5.2.2 Numerical Simulation

The model is simulated forward in time. Time steps are either equal to $\mathrm{d}t_{\max}$, the maximum time step the system can undergo, or they are determined through the Gillespie-style algorithm if the next motor state-change event (i.e., bound or unbound to microtubule,

ADP released or unreleased), also determined by the Gillespie-style algorithm, occurs before $t_n + \mathrm{d}t_{\max}$. An appropriate $\mathrm{dt}_{\max}$ (0.004) was chosen with a convergence test (Figure A.8). To implement the Gillespie-style algorithm, exponential random variables from distributions with means set by each Poisson (Equations 2.7, 2.8, 2.9 and 2.10) were generated at each time step. After the Gillespie-style algorithm determines the next event and when it occurs, the time step is used to determine the locations of the cargo center and the motor's head and anchor (Equations 2.4, 2.5 and 2.6).

Table 2.4: Hyperparameters for priors used in estimated posterior densities, all taken to be lognormal distributions.

Parameter	Mean	Standard Deviation
$k_{\text{off}}^{\text{ADP}}$	10^{-2}	0.001
$k_{\text{on}}^{\text{ADP}}$	10^{3}	100
$k_{\text{off}}^{\text{ADP,Fast}}$	$10^{0.3}$	1
$k_{\text{on}}^{\text{MT}}$	$10^{1.7}$	100
$k_{\text{off}}^{\text{MT}}$	10^{-1}	0.01
D_m	$10^{3.3}$	100
κ_w	$10^{-2.7}$	0.001

To mimic experimental practices, simulations are allowed to simulate 100 seconds. If the motor does not strongly bind to the microtubule during this time, the simulation starts over. This method is similar to the experiment, where the assay is run for 100 seconds screening for a binding event to occur before trapping a different cargo. The simulation is written in `MATLAB`, and takes approximately 0.1 seconds to simulate 1 second of the system. Example snapshots of the simulation are shown in (Figure A.1).

2.5.3 Model Fitting, Cross-Validation

The model is fit through two distinct approximate inference procedures, the reconciliation of which serves as a validation for the approximations. The first procedure is a Bayesian optimization procedure [1] to obtain a single point estimate for the parameter values. The loss function is the squared distance over the mean binding times (and therefore neglects the full distributional information) and the estimated mean binding time over $S = 1000$ simulations, and these estimates are used in Figure 2.2 and Table 2.1.

To obtain uncertainty quantification seen in Figure 2.4, we also employ a sequential Monte Carlo approximate Bayesian computation approach [103]. These techniques are far slower than the optimization procedure and require the specification of a prior distribution for each parameter, but provide some notion of uncertainty quantification, and were used to generate Figure 2.4 with some data withheld. That is, because of the heavy computation expense, only the shortest motor at 0 nm average distance between the cargo and microtubule, the mid-length motor at 40 nm average distance, and the longest motor at 80 nm average distance were used in the fitting. The maximum a posteriori (MAP) estimates from this latter procedure closely agree those of the first procedure, supporting the validity of both. Furthermore, in Table A.1, we show the inference procedures successfully infer rates from synthetic data. Lognormal priors are chosen for all parameters, and hyperparameters are shown in Table 2.4. Hyperparameters were chosen based on the range of values reported in the literature for each parameter when available. Otherwise, they were chosen to be approximately uninformative with large standard deviations. Initially, 100 simulations estimate the binding times in the model, and weights in the sequential Monte Carlo algorithm are defined as $w_i = \pi/(\sum w_{i-1}K_i)$, where K_i is the perturbation kernel for the ith sequence, $i > 1$. We use a Gaussian distribution for K. These new samples are then used to simulate more mean binding times until 100 samples are generated resulting in a relative error lower than 1.8. Eight more sequences follow in this same manner, each time the relative error threshold

decreases by 0.2. A kernel density estimator was then applied to the resulting samples shown in Figure 2.4.

The cross-validation procedure in Figure 2.2 was implemented by fitting the models using the aforementioned point estimate optimization scheme with data withheld, and then test error defined to be $N^{-1}\sum_{i=1}^{N}(t_i-\hat{t}_i)/t_i$, a percentage error over the test scenarios. This procedure is validated in Figure A.9 showing cross-validation successfully identifying the correct model when tested against synthetic data.

2.5.4 Software Availability

MATLAB code to reproduce our results (compatible with version R2020a) is available at `https://github.com/trininguyen/MotorBinding`.

Chapter 3

Computational modeling reveals a catch-and-guide interaction between kinesin-1 and tubulin C terminal tails

3.1 Abstract

Protein-protein interactions make up a very large bulk of cellular activity; however, they are still not very well-understood. Each of these interactions vary in their physical configurations (e.g. average distance from each other) and their tunable properties (e.g. reaction rates), which make them very difficult to study. One example of these interactions are the proteins on the microtubule surface interacting with motor proteins to control traffic on these filaments. Previous research has found that tubulin C terminal tails on the microtubule affect intracellular transport; specifically, cleaving these tails from the microtubule results in both shorter motor runlengths and slower velocities, suggesting that they assist with motor processivity and velocity on the microtubule, but it is not clear how this assistance happens.

In this work, we explore the different stages in the kinesin motor step cycle in which the tails can assist with both motor runlength and velocity. We consider three possible models: catching detaching motors, guiding the motor head's search for the next microtubule binding site, and stimulating ADP release. Using stochastic simulations and model fitting, we find that guiding the motor head's search for the next microtubule binding site is the most probable model of the tails' assistance, as this model fits all of the experimental data used, whereas the other two models cannot be fitted to the data with reasonable parameters. This work provides insight into motor-CTT interactions that currently cannot be observed in experiments. Understanding this interaction is essential in understanding other integral details of transport, such as post-translational modifications on CTTs and the tubulin code that regulates microtubule traffic. By fully understanding the mechanisms by which all of the many components in transport use to interact with each other, we can further understand the requirements of a healthy cell and advance cell therapies accordingly.

3.2 Introduction

Numerous protein-protein interactions take place within cells, with each interaction subject to being modulated by the cell itself (e.g. via post-translational modifications and protein concentrations) [111]. These modulations increase the number of potential reactions and processes in the cell, making understanding these interactions difficult, and even with specific measurements of these interactions, it is difficult to integrate the complexity into predictive models. One such interaction involves intracellular cargoes, such as lipid droplets or mitochondria, engaging with microtubules via motor proteins to be transported to their needed locations in a timely manner [33]. Efficient intracellular transport is vital for cellular function. Motor proteins, such as kinesin, facilitate this transport by binding to the cargoes and transporting them along microtubules [114]. However, this is no simple feat. The traffic on

microtubules is fairly complicated, as there are different types of motor proteins that travel in opposing directions. In addition to these motor proteins, other microtubule-associated proteins, such as tau and MAP-7, take up space on the microtubule surface, and motors must carefully navigate through this crowded traffic. The different cargoes that motor proteins transport also differ in shapes and sizes, adding to the highly complex traffic. Due to this complexity, a holistic understanding of transport is still yet to be acheived. The effects of understanding this process extends outside of this process itself. Because this system plays an important role in cell biology with combinatorial complexity and it is manipulatable via single-molecule studies [10, 51, 79, 98, 101, 104], the intracellular transport system offers a valuable model for studying protein-protein interactions as well.

Despite the intense complexity on microtubules, the cell can impressively regulate motor protein traffic using the "tubulin code", in which post-translational modifications are performed on specific areas of the microtubule, affecting the recruitment of proteins at specific moments [46] or areas of the cell [39, 52]. With this control, the cell can transport several different cargoes simultaneously. Most of the post-translational modifications are made on tubulin C terminal tails (CTTs), which extend from each tubulin monomer on the microtubule [80]. The role of CTTs, with or without modifications, on microtubules is unclear, mostly because the affect of these tails vary greatly between different motors they interact with and whether the tail came from an α or β tubulin monomer [94, 61], and this variation makes understanding CTTs difficult. But, they are part of the cell's "tubulin code", which has been evident in experimental results that show their affect on transport [24]. For example, an experimental study from [102] found that cleaving the CTTs from microtubules results in shorter processivity and slower velocity for the motor protein kinesin-1, suggesting that CTTs (without any modifications) can modulate the kinetics of at least some motor proteins. However, the mechanism by which CTTs can aid these motors on the microtubule remains unknown, since it is difficult to directly observe the mechanisms that control motor stepping. While experiments can measure how far and fast motors walk on the microtubule,

they cannot reveal the different conformational states the motor undergo in order to make stepping possible. This challenge must be overcome in order to further our understanding of the interactions between a CTT and a motor, which we can then use to understand the CTT post-translational modification effects on transport and the functionings of a healthy cell. Modeling and computational simulation may by helpful in overcoming this challenge and providing insight into CTTs where experiments cannot, specifically by integrating mathematical models with existing knowledge of these motor states.

Here, we use a computational approach to explore possible models of the contribution CTTs can provide to kinesin-1's processivity (Figure 3.1). Specifically, we are interested in a model that can reproduce CTTs lengthening motor processivity *and* speeding up velocity, with a reasonable parameter regime. Deriving such a model is not straightforward, as there are models that suggest CTTs lengthen motor processivity but slow down its velocity, or that they make motors faster but fall off the microtubule sooner. There are also models that can explain both results, but with an unrealistic parameter regime. We consider three different models in hopes that one could satisfy *all* of those conditions: (1) CTTs catch motors that unbind from the microtubule, (2) they guide the motor head's diffusive search for the next microtubule binding site during stepping, and (3) they stimulate ADP-release similarly to microtubule-stimulated ADP release [104]. Each of these models, at first thought, seem equally plausible to explain the perplexing result in [102], as they seem to satisfy at least one of our three modeling requirements. To carefully explore these models, we computationally simulate these models by expressing them as Markov chain models and fitting their unknown parameters to experimental data from [102]. After this analysis, we find that the "catch" model could not explain both processivity and velocity experimental data simultaneously, since the model could theoretically result in an extension of runlengths, but the mechanism would slow down motor stepping, instead of speeding it up as seen in experiments. We also find that the third model could not predict processivity on cleaved microtubules with reasonable parameters. However, the second model matches all of the available observed

data, which makes this model a strong candidate that can explain the role of CTTs. Not only can this model explain the result from [102], but it may also explain why CTTs are positioned close to binding sites on the microtubule [46].

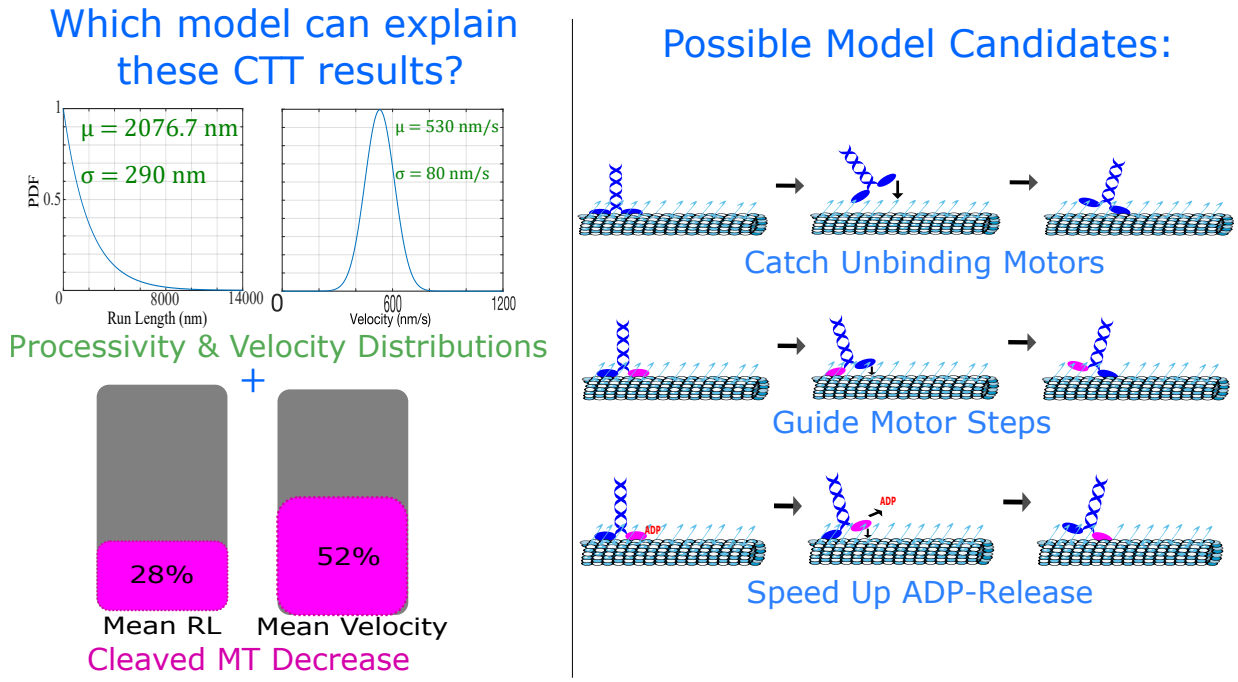

Figure 3.1: Possible CTT Mechanisms for Motor Processivity Assistance. Left: The ideal model that can explain how CTTs can assist motors on microtubules will need to explain all of the displayed data, with physiologically feasible parameters. Right: Possible models explored that may explain the data. First model: CTTs catch motors as they unbind from the microtubule and pull them back. Second model: One of the motor's head is dangling as it searches for a microtubule binding site to take the next step. CTTs help guide this dangling head to that next binding site. Third model: CTTs speed up ADP release.

3.3 Results

3.3.1 By catching unbound motors, CTTs can extend their runlengths on the microtubule, but would also slow them down in the process.

We simulate a motor (not bound to any cargo) walking on the microtubule using a Gillespie algorithm [30]. This simulation includes the model of the kinesin-1 step-cycle in existing literature [69], so ADP, ATP, and phosphate release and binding are all involved (Figure 3.2). This general model of kinesin stepping is as follows: one of the motor's head strongly binds to the microtubule when it comes into contact with the microtubule *and* ADP is released from that head. ATP then binds to this head, which results in a change of orientation in which the other head now switches forward. This head now needs to come into contact with the next binding site on the microtubule and await ADP release to finish the motor's step. If phosphate release on the bound head happens before ADP is released from the front dangling head, then the motor becomes unbound. This model does not include interactions between a CTT and the motor. To consider CTTs assisting the motor, we included another state (State 9 in Figure 3.3a) to this model, where it is possible for a CTT to catch the motor as it unbinds from the microtubule and hold it until it can rebind to the microtubule. Most of the parameters were taken from estimates in the existing literature (Table 3.1). The unknown parameters of this model were then fitted to the experimental data from [102], which included distributions of runlength and velocity of motors on wildtype microtubules and fold comparisons of mean runlength and velocity of motors on microtubules with CTTs cleaved compared to motors on wildtype microtubules. With the addition of the "caught state", State 9, we hoped that this catching mechanism would allow the motor to walk on the microtubule further than when CTTs are absent, as seen in [102], and indeed we were able to fit this model to the experimental processivity results (Figure 3.3b), and there does seem to

be a processivity advantage that CTTs provide to motors (Figure 3.3c). Thus, by catching motors, CTTs can decrease unbinding events and the motors can stay on the microtubules longer, resulting in longer runlengths. However, the model's velocity did not match that of the experimental data (Figure 3.3d), since there is an additional state in the model that does not provide any method for faster runs. Thus, it is not likely that CTTs can help motors by only catching them before they unbind from the microtubule.

3.3.2 Guiding dangling motor heads close to the next microtubule binding site results in an increase in both runlength and velocity.

Since the catching mechanism does allow for longer processivity, we opted to retain it in the next model that we explored. To speed up velocity, we predict that CTTs interact with the motor earlier on in the kinesin step-cycle, while the motor is still very much bound to the microtubule. Specifically, when one motor head is bound to the microtubule, the other is unbound and searching for the next binding site to take its next step. In this unbound position, the motor may bind to a nearby CTT, and since CTTs are very near microtubule binding sites [46], the CTT could speed up this dangling head's diffusive search for the next binding site by guiding this head to that site. Figure 3.4a shows the different states of this model, where a CTT binds to the dangling motor head in State 9 and guides it to the microtubule in State 7. A speed up in velocity would require for the transitions from State 6 to 9 then 7 be overall faster than the transitions from 6 to 7. The catching mechanism from Figure 3.3 is now in State 10, where if the bound head becomes unbound, the CTT still holds on to the motor. However, this model does not need to solely depend on State 10 to extend runlengths, as the addition of State 9 allows for another possible state the motor can enter from State 6 that is not back to State 2 (and subsequently, detachment

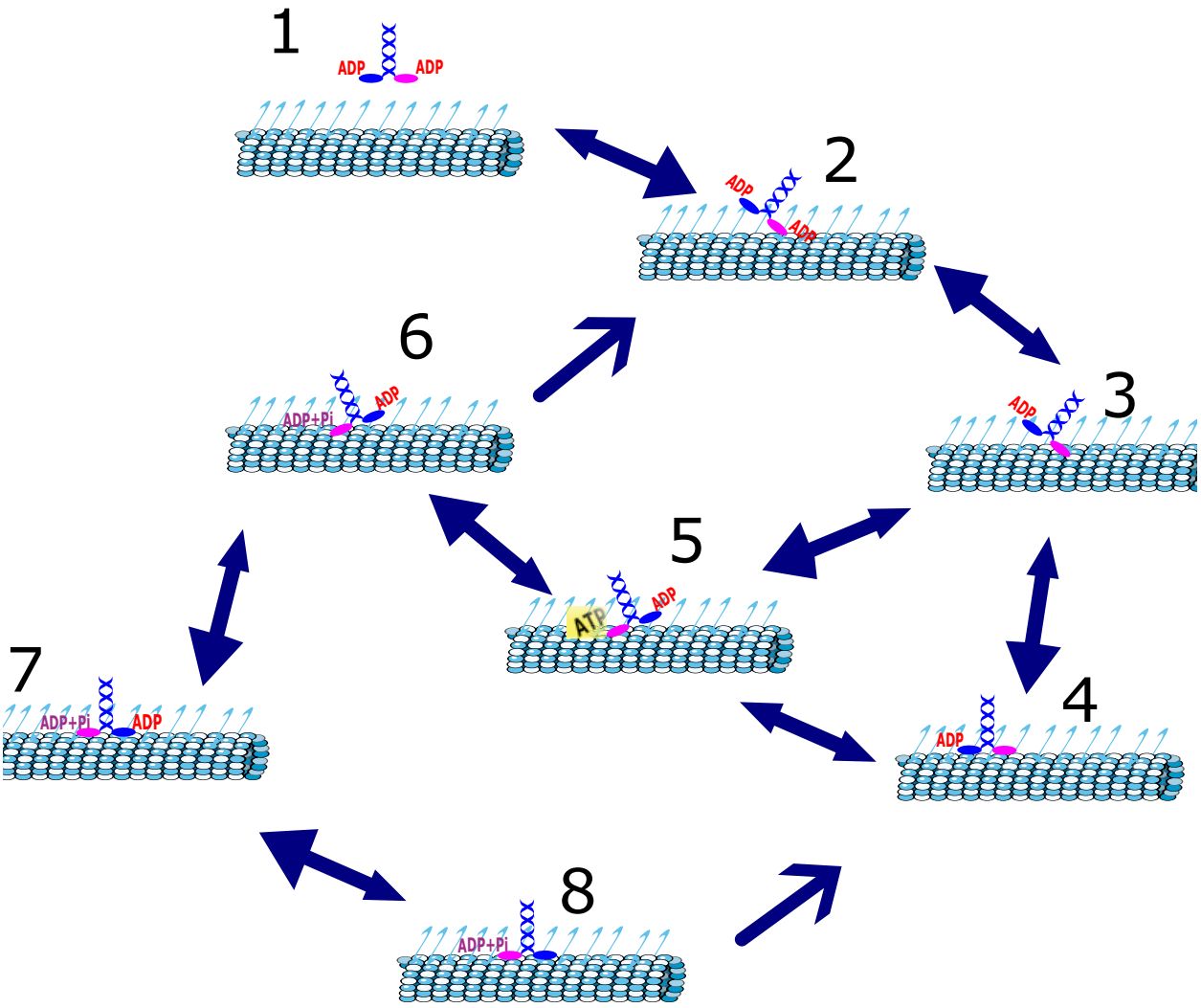

Figure 3.2: Model of Kinesin Stepping in Existing Literature. Current models of stepping do not consider the motor's interaction with the CTT. The motor can strongly bind to the microtubule when ADP is released from the microtubule-bound head (State 3) [69]. ATP binding to this head results in the trailing head (blue head) switching forward (State 5). ADP-release from this head results in another strong binding to the microtubule (State 8), which allows the motor to finish taking one step.

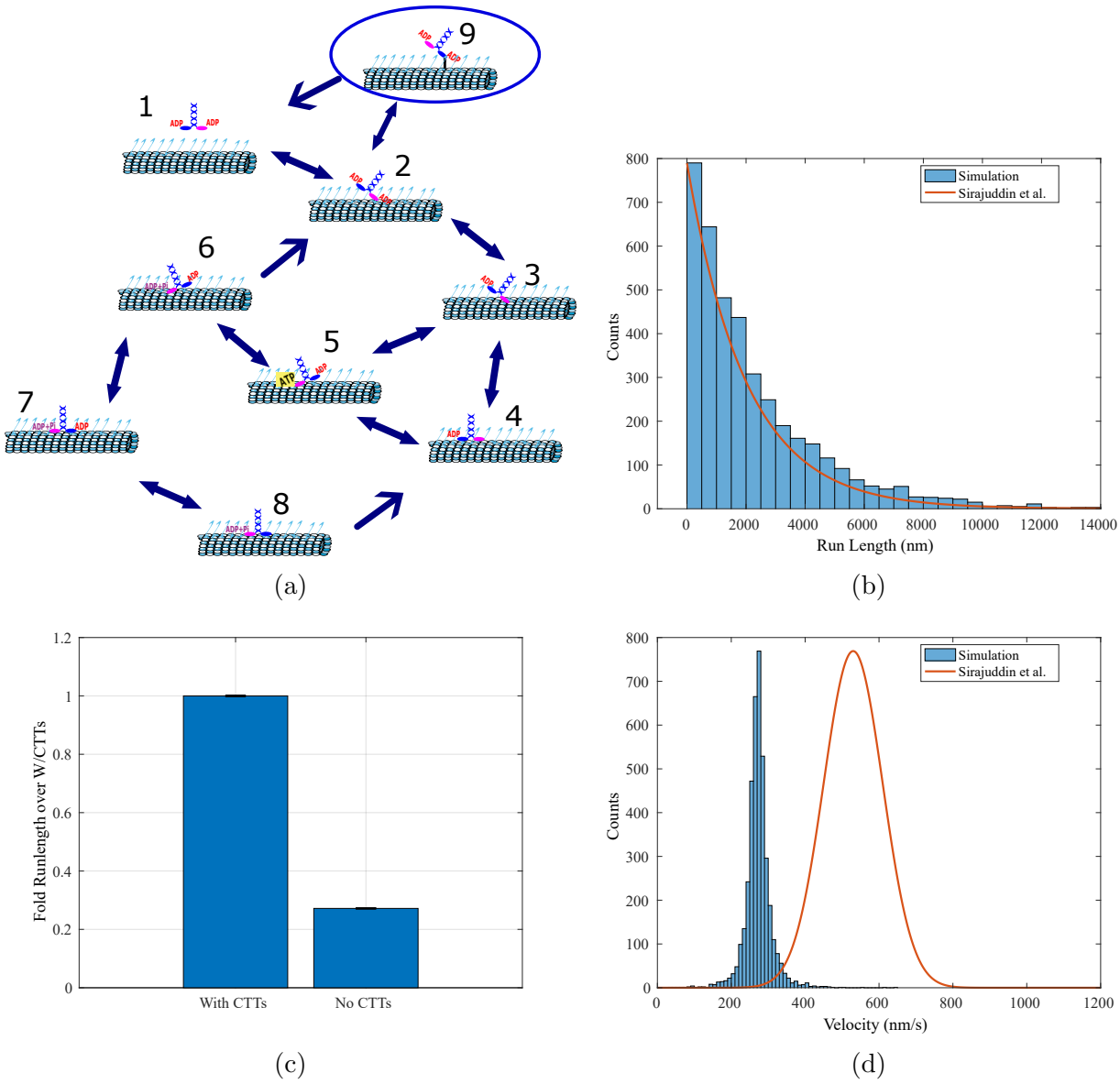

Figure 3.3: Catching motors results in longer run lengths but slower velocities. (a) This model is similar to Figure 3.2, with an additional state (State 9) that considers the CTT catching unbound motors. The model can recapture observed runlengths (b) but fails to do so for velocity (d). $n = 4000$ simulations using parameters from Table 3.1. Red curves are wildtype (with CTTs) data from [102]. (c) Mean runlengths for the model in (a) (with CTTs) was taken from 4000 simulations. Mean run lengths from the model in Figure 3.2 (with CTTs cleaved from the microtubule) were then compared to these means. $n = 3 \pm$ SEM.

to State 1). From Figure 3.4f, we can see that this model indeed does not enter State 10 much, and thus does not rely on it to fit to observed runlengths. We also considered a model that considers only the guiding mechanism without any catching assistance (Figure B.1), and this model's predictive power was comparable to the Catch+Guide model, with no significant difference in the predictive errors. The Catch+Guide model was able to match both the experimental data's runlength and velocity (Figure 3.4b and c). In addition, the fold differences in runlength and velocity between setups with CTTs and those with cleaved CTTs also match those that were previously observed [102] (Figure 3.4d and e). Thus, CTTs acting as a guide for dangling motor heads to the next microtubule binding site is a compelling and likely mechanism.

3.3.3 The model that considers CTTs stimulating ADP release cannot explain experimental data with reasonable parameters.

Previous studies have found that when both kinesin motor heads bind to the microtubule, the tubulin from the microtubule stimulates ADP-release at a faster rate of $\sim$120 s^{-1} [37, 100]. Since CTTs are essentially made up of tubulin, we wondered if the CTT could also stimulate ADP release from the motor heads. To explore the possibility of this mechanism, we allowed in our simulations for ADP-release to occur at a stimulated rate if the motor binds to the CTT, as well as when it binds to the microtubule (Figure 3.5a). Since the previously estimated release rate of $\sim$120 s^{-1} was obtained from experiments using wild type microtubules (with CTTs), the release rate for microtubules with cleaved CTTs may be slower to result in slower motor velocities. Thus, to evaluate the predictive power of this model, we first fitted the unknown motor-microtubule binding rate, motor-CTT binding rate, and motor-CTT unbinding rate to the wild type processivity and velocity data, using a fixed stimulated

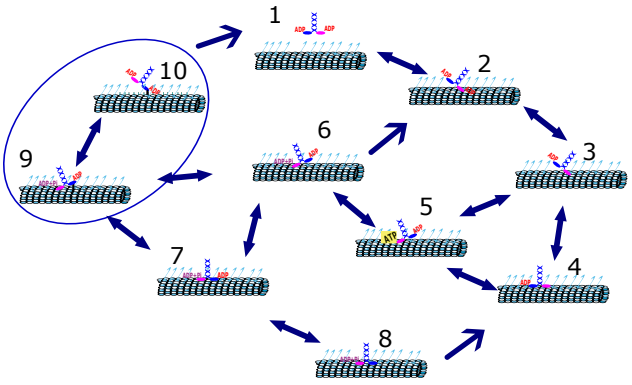

(a)

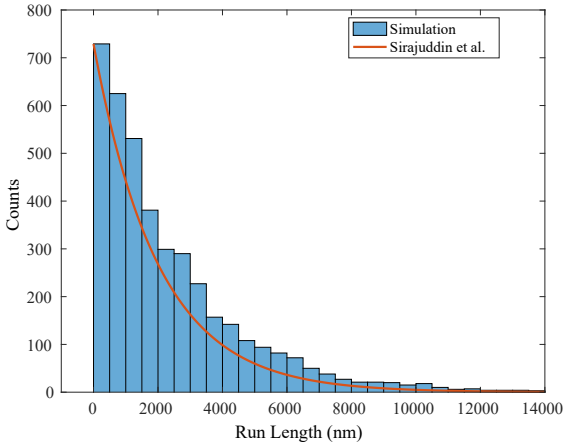

(b)

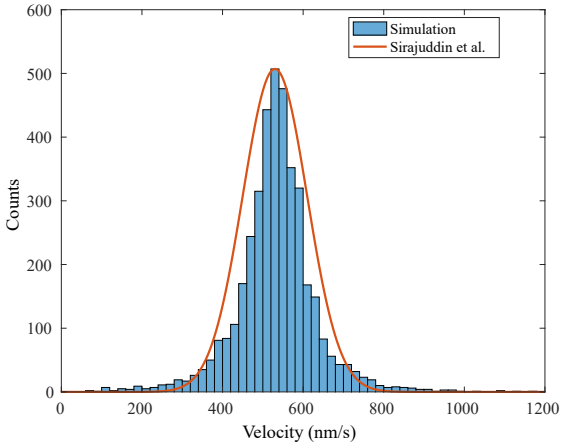

(c)

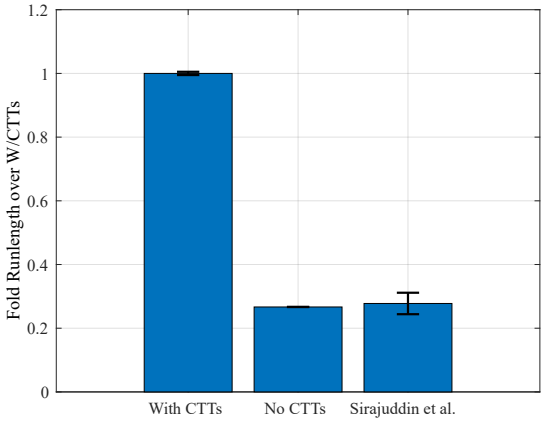

(d)

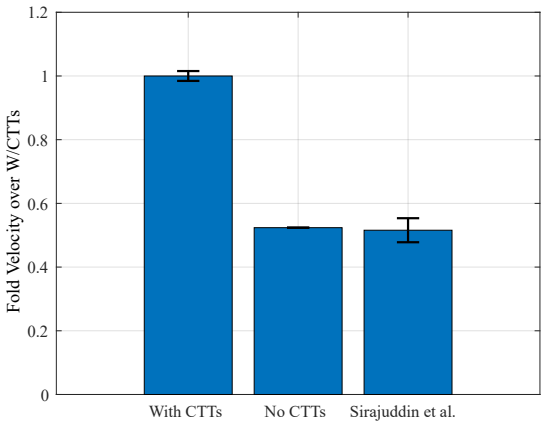

(e)

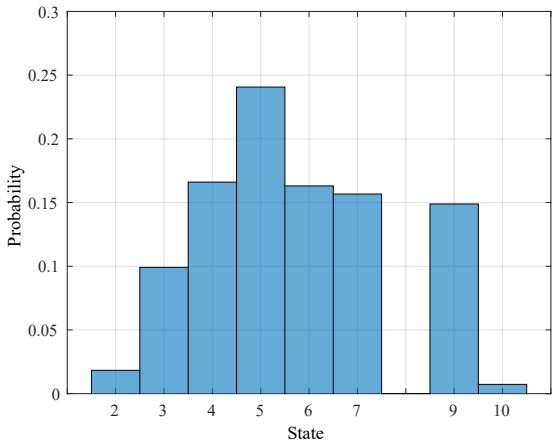

(f)

Figure 3.4: CTTs guiding dangling motor heads to the next microtubule binding site model matches both experimental runlengths and velocities (Continued on the following page.)

Figure 3.4: (a) A CTT binds to the unbound motor head while the other motor head is bound to the microtubule (State 9). The CTT can then guide it to the next microtubule binding site, ideally speeding up its search for this site. The catching mechanism is still considered in this model (State 10). (b and c) Experimentally observed runlengths (red curve, b) and velocities (c) [102] over computationally simulated runlengths and velocities (blue bars) from motors on wildtype microtubules (with CTTs). $n = 4000$ simulations. (d and e) Runlengths and velocities presented as ratios over that of the setup with CTTs, as mean $\pm$ SEM, $n = 3$ runs of 4000 simulations each. Third bars are ratios of motors on cleaved microtubules data over motors on wild type microtubules from [102]. (f) Probability of a motor being in a certain state in the model at a given time. States 8 and 4 are the same and thus grouped together under State 4.

ADP-release rate of $\sim$120 s^{-1}. We then fitted the unknown slower stimulated ADP-release rate for cleaved microtubules to the cleaved microtubule experimental velocity data, with fixed values for the motor-microtubule and -CTT binding and motor-CTT unbinding rates, obtained from the previous fit with the wild type data. To obtain reasonable fits with the experimental velocity, this slowed-down rate had to be decreased by about 50% (Table 3.1). With these fitted values, we predicted the cleaved microtubule experimental processivity data (Figure 3.5b). This prediction resulted in no decrease in runlength, which does not match the experimental data. We then tried to slow down the unloaded (one-headed) stimulated ADP-release rate that occurs from States 2 to 1 in the cleaved microtubule simulations as well. Since the fitted loaded rate decreased by about 50%, we lowered the unloaded rate to the same magnitude. By doing so, we retained the match in velocity, so the loaded rate does not affect velocity. We also observed a reduction in processivity; however, the reduction was not enough to match the experimental data. Thus, it is not likely that CTTs can assist motors solely by stimulating ADP-release.

3.4 Discussion

Previous work has indicated that CTTs help extend kinesin-1 processivity and quicken its velocity. Our computational results ruled out some possible models of the CTTs assisting

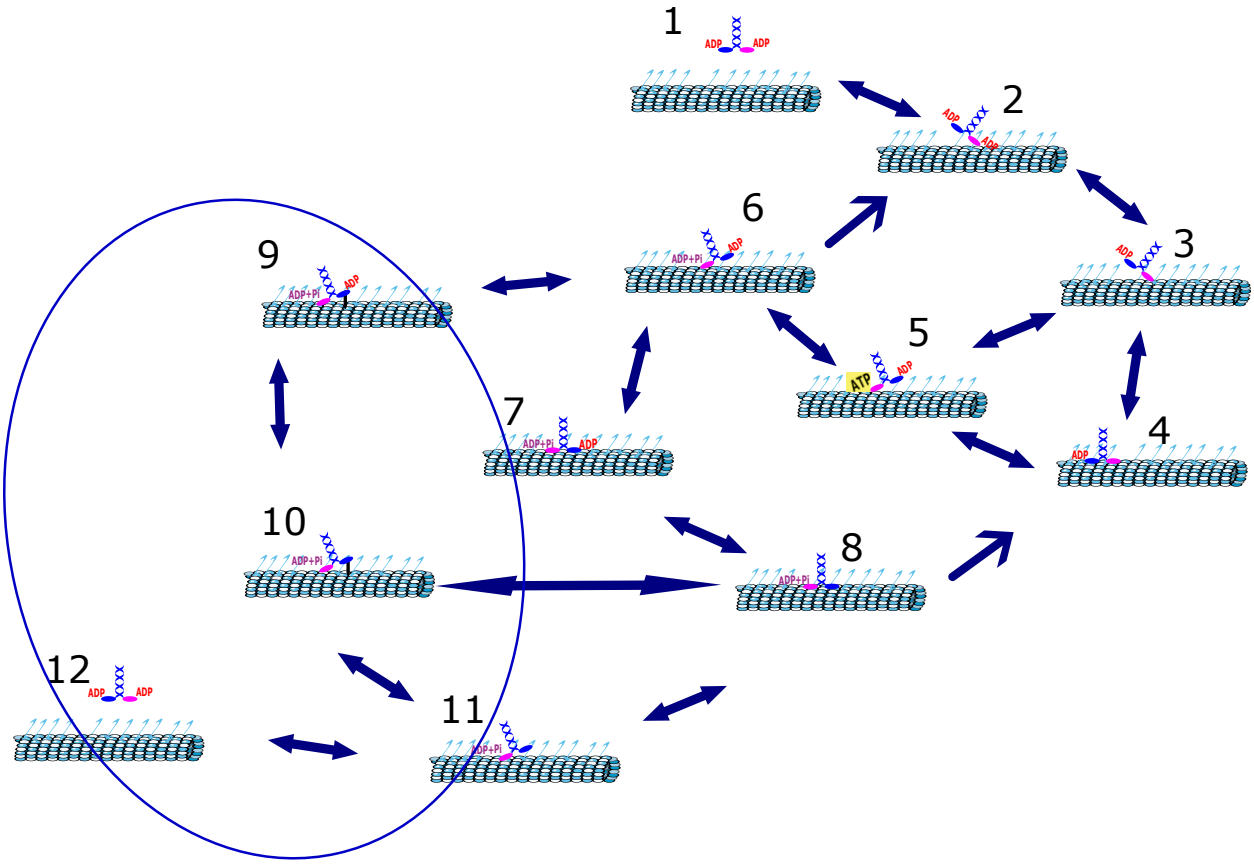

(a)

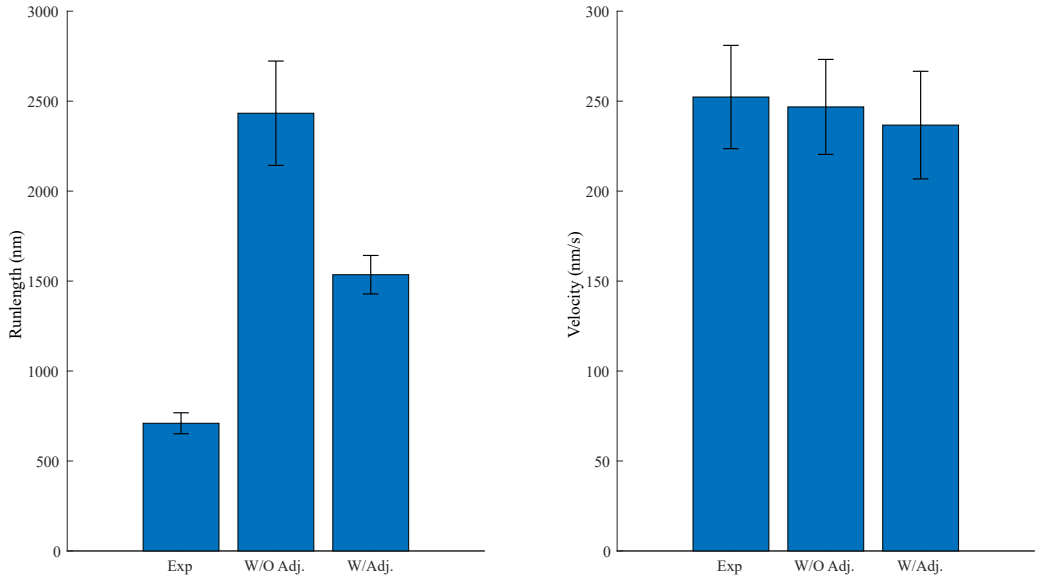

(b)

Figure 3.5: CTTs stimulating ADP release model cannot explain data with reasonable parameters. (a) Diagram of model. (b) Fitted model results does not match experimental data, even when the unloaded ADP-release rate from State 2 was adjusted.

motors on the microtubule. The catching model and the ADP-release model could only fit to either experimental processivity or velocity data, but they could not fit both. However, simulating CTTs guiding dangling motor heads to their next microtubule binding site allowed for successful fitting to all experimental data used. This model could also explain experimental results from other studies; for example, the lack of guiding assistance from the CTTs could explain the result in [112], in which the authors have found that cleaving the CTTs increases backstepping, which may be more likely to happen without the CTT pulling the motor head forward. Thus, we believe this model can explain at least partially the role of CTTs on microtubules.

The fitted parameters from our models provide further support of the CTT-guiding model (Table 3.1). For example, extremely high rates had to be utilized to allow the CTT-catch model to fit experimental processivity data; however, despite the high motor-microtubule on-rate, the velocity predicted by this model is still much lower than the observed data. Theoretically, the parameters in the ADP model can be tuned further to result in a closer fit to the experimental data; however, we do not believe the extent of the tuning is physiologically feasible. Specifically, we believe the unloaded ADP-release rate in the cleaved microtubule case should be decreased the same magnitude as the loaded rate. We believe we chose a fairly low motor-microtubule on-rate, since inference shows that the possible values for this parameter can be high for this model to fit the experimental velocity (Figure B.2). In contrast, the fitted parameters from the CTT-guiding model are more reasonable and not extreme.

While the relationship between motor proteins and microtubules has been extensively studied, much is still unknown about the role of CTTs. Understanding the mechanisms that CTTs use in intracellular transport will provide insight into post-translational modifications made on the microtubule as part of the tubulin code [46]. Many studies are currently focused on attempting to understand these post-translational modifications and their impact on a

healthy cell [14, 121, 5, 118], and most of these modifications occur on CTTs [46]. Therefore, to fully understand the impact of these modifications, it first must be understood how CTTs behave without any modifications. Specifically, more experiments need to be conducted to observe CTT behavior. For example, an experiment can confirm our CTT-guiding model, perhaps by measuring the movement of the unbound leading motor head of motors on wildtype microtubules vs. cleaved microtubules via light-scattering methods [47]. In this experiment, a result of the motor head's position concentrated in a specific area on wildtype microtubules, and the motor head's position scattered on cleaved microtubules, would validate our model. Even without experiments, we can still use computational methods to eliminate other CTTs models, which further supports the possibility of our CTT-guiding model.

It is important to note that we believe our model applies specifically to kinesin-1, in which this kinesin's positively-charged areas on its motor domains have a weak attraction to the negatively-charged CTTs [109]. Namely, the parameter regime that resulted from our model fitting is specific to kinesin-1. A different computational study for dynein has posited a similar model in which the CTT guides dynein motor heads to the microtubule [108]. Other studies have found that CTTs (without any post-translational modifications) may not assist other motors [102, 61], possibly also due to electrostatic incompatibility [34], but post-translational modifications can change the charge of the CTTs, controlling how the CTTs can affect motor processivity. Although CTTs may not assist these motors, their absence do have an effect on the motors [102], and the mechanism for these effects are not understood. Future studies can use our approach of combining computational models of processivity and velocity measurements with the motor stepping cycle to pinpoint where CTTs may influence motor behavior.

Altogether, at first thought, each of our explored models seem very plausible in explaining the role of CTTs. Using theory, we can take a closer look at these models and eliminate

those that cannot be justified statistically. Our remaining model can be confirmed through experiment, making a combined theoretical-experimental approach very effective in studying cellular behavior.

3.5 Methods

3.5.1 Simulation

We simulate an unbound kinesin-1 motor diffusing to a microtubule, binding to it, and walking on it. Transitions between each state are modeled as Poisson processes, with rates from Table 3.1. These transitions are simulated using a Gillespie algorithm [30]. At each time step, the time to the next step is computed as

$$\Delta t = \frac{1}{\sum r_i} \cdot \ln \frac{1}{w_1},$$

where r is the rate of the ith reaction and w_1 is a random number between 0 and 1. To determine which reaction will occur at $t + \Delta t$, we find the smallest integer i that satisfies

$$\sum_{i'=1}^{i} r'_i > w_2 \sum_i r_i,$$

where w_2 is another random number between 0 and 1. We take runlength to be the entire length the motor walks on the microtubule until it falls off completely from the microtubule (the motor unbinds from the microtubule and a CTT). We take velocity to be this runlength over the total time the motor was on the microtubule. The simulation is written in Matlab.

Table 3.1: Parameters Used in Simulations. MT: microtubule, WT: wildtype

Parameter (s^{-1})	Catch	Catch & Guide	Stimulated ADP-release	States, Citation
Motor-MT on-rate	1.8e4	410	3973	1 to 2, 3 to 4, 6 to 7, Fitted
Motor-MT off-rate	0.7	0.7	0.7	2 to 1, 4 to 3, 7 to 6 [10, 116, 123, 62]
Motor-CTT on-rate	2.6e6	767	437	2 to 9 in Catch, 6 to 9 in Catch+Guide and ADP, 11 to 10 in ADP, Fitted
Motor-CTT off-rate	548	76	370	9 to 1 in Catch, 9 to 6 and 10 to 1 in Catch+Guide, 9 to 6 and 10 to 11 in ADP, Fitted
Motor-MT CTT-assisted on-rate	-	510	-	9 to 7 in Catch+Guide, Fitted
Loaded ADP off-rate	120	120	120 for WT; 50 for cleaved	7 to 8, 9 to 10 in ADP, Fitted for ADP [37, 100]
Unloaded ADP off-rate	2	2	2 for WT; 0.8 for cleaved	2 to 3, Fitted for ADP [37, 100]
Phosphate on-rate	0.001	0.001	0.001	6 to 5 [95]
Phosphate off-rate	100	100	100	6 to 2 [19]
ATP on-rate	4000	4000	4000	3 to 2, 8 to 7, 10 to 9 in ADP [19]
ATP on-rate	100	100	100	3 to 5, 4 to 5 [19]
ATP hydrolysis rate	200	200	200	5 to 6 [19]

3.5.2 Model Fitting

To infer the parameters of our models, we fit all models to experimental data from [102] using a simple approximate Bayesian computation algorithm [103] and selecting the parameters that resulted in the smallest absolute error (maximum a posteriori estimate). Uniform priors were used. The available data consisted of processivity mean and variance, velocity mean and variance, and fold comparisons of the cleaved microtubule cases for both processivity and velocity means. The cross-validation analysis (Figure B.1) was performed similarly, but only using the velocity data for training and subsequently the processivity data for testing. The simple approximate Bayesian computation algorithm is as follows:

while $n \leq N$ **do**

Sample θ^* from prior $\pi(\theta)$

for $i = 1$ to N **do**

Determine predicted runlengths and velocities using θ^*

end for

Calculate mean and variance of predicted runlengths and velocities

Calculate absolute error between predicted and experimental values

end while

Take θ^* that resulted in the smallest error.

To produce Figure B.2, the above algorithm was used on the ADP-release model and the parameters that resulted in the lowest 1% absolute error were chosen. Only experimental data from the wildtype microtubules were used.

Chapter 4

Summary and Conclusions

By studying the motor interacting with the microtubule and CTTs, we not only gain more insight into the complex intracellular transport system, but we also learn how we may study other similar complex biological systems. Specifically, this dissertation provides examples of how we may use computational models to study mechanisms that currently cannot be observed through experiments. We have presented multiple mechanisms in which the motor may use to perform effective intracellular transport on the microtubule, and we have provided thorough analyses of the plausibility of each of these mechanisms. The motor's involvement in intracellular transport is essential for healthy cellular function; therefore, a thorough understand of the motor's interactions with the microtubule is pertinent. The motor mainly interacts with the microtubule in three ways, two of which are binding (discussed in Chapter 2) and stepping (discussed in Chapter 3). In both chapters, we consider models that vary in mechanisms and number of states within a model, and the race of reactions in which these mechanisms may occur. These interactions occur at a very microscopic scale and thus are very difficult to observe via experiments. However, we have shown that by combining the data that we can collect with theoretical and computational analyses, we can deepen our understanding of these complicated and miniscule systems. Thus, we are presenting a

holistic analysis on a biological system and an example of how other complex systems can also be studied.

4.1 Complex motor-microtuble binding

The motor binding to the microtubule is arguably the most important process in intracellular transport since it is the very first process of transport. Of the three major processes of transport (binding, walking, and unbinding), binding happens to be the most difficult process to understand and observe, mainly due to the difficulty in disentangling all of the mechanisms that occur immediately before and after binding. Specifically, it is difficult to pinpoint the exact moment that binding occurs. It was previously assumed that binding occurs very simply and that the only significant mechanism involved in binding is the motor diffusing to the microtubule. However, our single-molecule measurements have shown that simple diffusion is not a likely model for binding, especially because simple diffusion cannot explain the observed binding delay that occurs when the motor does not need much diffusion to come into contact with the microtubule. This finding motivated us to rethink the binding process and consider whether there are other subprocesses that may be rate-limiting and significant. While we presented compelling support for the accelerated ADP-release rate model, we believe the more significant result from this work is that motor-microtubule binding is not simple and is a multi-step process.

We approached this problem by electing to control the spacing between the cargo and microtubule *in vitro*. *In vivo*, this spacing is also varied depending on the proteins covering the microtubule surface that the cargo is diffusing towards. Some proteins will pull the cargo closer to the microtubule [4], and others will push the cargo away [56]. With our results, we have predicted the time scales at which the cargo will bind to the microtubule in each of these cases. These estimated time scales give insight into the results of the microtubule's

tubulin code, and perhaps the goal and purpose of this code. The effects of spacing between two interacting proteins is not unique to the intracellular transport system. Cell-signaling-involved proteins that need to be recruited to tethered proteins on the cell surface also face the problem of having their targeted binding sites obscured by the crowding effects of neighboring proteins [32]. The methods used in this work could be applied to study the complex traffic system at the cell surface as well.

4.2 CTT assistance with physical search during stepping

Once the motor successfully binds to the microtubule, it must walk on it for several steps (about 250 steps for kinesin-1 [2]) in order to transport the cargo to its needed destination. With extreme traffic on the microtubule, how can the motor succeed in making so many steps with the odds stacked against it? Experimental results suggested that CTTs may provide assistance to these motors; however, these results are not straightforward. According to these results, the tails can help the motor stay on the microtubule *and* allow to it transport its cargo in a very timely manner. It is not obvious how the tails achieve this feat. For example, we were initially very confident in the potential of the Catching model that we explored. In this model, CTTs definitely keep the motor on the microtubule for longer runlengths. However, as seen from Chapter 3, the model could not explain CTTs speeding up the motors. Thus, this problem was not trivial.

The difficulty in not being able to observe the CTT-motor interaction directly in experiments and the non-trivial manner of the problem makes modeling an ideal method to study CTTs. Some CTT interactions cannot be observed in experiments, and the interactions that can be observed require methods that are very energy-, material-, and time-consuming, and it is not

obvious which experimental methods are best to study these tails. It is very possible that after months of experiments, it would finally be apparent that the results are inconclusive. There is also the issue that a hypothesis may prove itself to fail in an experiment, and so more experiments need to be conducted to test other hypotheses. However, using computational methods can speed up the process of exploring different hypotheses. In addition, with the predictions from the models in our work, experimentalists can now more carefully select methods that would verify our models. Further modeling also needs to be completed to support our model, such as determining the strength and stiffness the CTT requires in order to pull on the motor head. This quantification would provide details into the CTT structure that are currently unknown. Therefore, computational methods must be combined with experimental methods to efficiently study these complex systems.

4.3 Conclusions

While intracellular transport has been extensively studied, this dissertation focuses on transport processes that involve details and steps that remain obscure to scientists. This has been accomplished by taking advantage of computational methods and combining them with experimental methods. Both methods alone have their weaknesses: there are limitations to what can be observed through experiments, and the insights gained from modeling remain as hypotheses until they can be proven and/or observed through experiments. However, if we attempt to model the limited experimental data, and subsequently test those models with more experiments, we can efficiently study complex biological processes.

Bibliography

[1] L. Acerbi and W. Ma. Practical Bayesian optimization for model fitting with Bayesian Adaptive Direct Search. *Advances in Neural Information Processing Systems*, 2017.

[2] J. Andreasson, B. Milic, G.-Y. Chen, N. Guydosh, W. Hancock, and S. Block. Examining kinesin processivity within a general gating framework. *elife*, 4, 2015.

[3] A. B. Asenjo, Y. Weinberg, and H. Sosa. Nucleotide binding and hydrolysis induces a disorder-order transition in the kinesin neck-linker region. *Nature structural & molecular biology*, 2006.

[4] S. Ayloo, J. Lazarus, A. Dodda, M. Tokito, E. Ostap, and E. Holzbaur. Dynactin functions as both a dynamic tether and brake during dynein-driven motility. *Nature Communications*, 2014.

[5] J. Bar, Y. Popp, M. Bucher, and M. Mikhaylova. Direct and indirect effects of tubulin post-translational modifications on microtubule stability: insights and regulations. *Biochimica et Biophyscia Acta-Molecular Cell Research*, 2022.

[6] N. N. Batada, L. A. Shepp, and D. O. Siegmund. Stochastic model of protein–protein interaction: Why signaling proteins need to be colocalized. *Proceedings of the National Academy of Sciences*, 2004.

[7] J. Berg, J. Tymoczko, and L. Stryer. Kinesin and dynein move along microtubules. *Biochemistry*, 2002.

[8] O. Berg. Orientation constraints in diffusion-limited macromolecular association. the role of surface diffusion as a rate-enhancing mechanism. *Biophysical journal*, 1985.

[9] S. Block. Kinesin motor mechanics: Binding, stepping, tracking, gating, and limping. *Biophysical Journal*, 2007.

[10] S. Block, L. Goldstein, and B. Schnapp. Bead movement by single kinesin molecules studied with optical tweezers. *Nature*, 1990.

[11] M. Bovyn, B. Narayanareddy, S. Gross, and J. Allard. Diffusion of kinesin motors on cargo can enhance binding and run lengths during intracellular transport. *Molecular Biology of the Cell*, 2021.

[12] M. Bovyn, B. Reddy, S. Gross, and J. Allard. Roles of motor on-rate and cargo mobility in intracellular transport. *bioRxiv*, 2020.

[13] K. P. Burnham and D. R. Anderson. Multimodel inference: understanding aic and bic in model selection. *Sociological methods & research*, 2004.

[14] L. Chen and A. Kashina. Post-translational modifications of the protein termini. *Frontiers in Cell and Developmental Biology*, 2021.

[15] C. Choi, C. Margraves, and K. Kihm. Examination of near-wall hindered brownian diffusion of nanoparticles: Experimental comparison to theories by brenner (1961) and goldman et al.(1967). *Physics of Fluids*, 19(10), 2007.

[16] H. Choi, M. Auley, and D. Lawrence. Prenatal exposures and exposomics of asthmas. *American Institute of Mathematical Sciences Environmental Science*, 2015.

[17] M. Ciocanel, B. Sandstede, S. P. Jeschonek, and K. L. Mowry. Modeling microtubule-based transport and anchoring of mRNA. *Society for Industrial and Applied Mathematics Journal on Applied Dynamical Systems*, 2018.

[18] K. Cranmer, J. Brehmer, and G. Louppe. The frontier of simulation-based inference. *Proceedings of the National Academy of Sciences*, 2020.

[19] R. A. Cross. The kinetic mechanism of kinesin. *Trends in biochemical sciences*, 2004.

[20] K. De Vos, A. Grierson, S. Ackerley, and C. Miller. Role of axonal transport in neurodegenerative diseases. *Annual Review of Neuroscience*, 2008.

[21] M. Dutta and J. B. Computational modeling of dynein motor proteins at work. *Royal Society of Chemistry*, 2021.

[22] J. Espeut, A. Gaussen, P. Bieling, V. Morin, S. Prieto, D. Fewquet, T. Surrey, and A. Abrieu. Phosphorylation relieves autoinhibition of the kinetochore motor cenp-e. *Molecular Cell*, 2008.

[23] X. Fan and R. J. McKenney. Control of motor landing and processivity by the CAP-Gly domain in the KIF13B tail. *Nature Communications*, 2023.

[24] M. Feizabadi, B. Reddy, O. Vadpey, Y. Jun, D. Chapman, S. Rosenfeld, and S. Gross. Microtubule C-terminal tails can change characteristics of motor force production. *Traffic*, 2015.

[25] Q. Feng, K. J. Mickolajczyk, G.-Y. Chen, and W. O. Hancock. Motor reattachment kinetics play a dominant role in multimotor-driven cargo transport. *Biophysical journal*, 2018.

[26] C. Friel and J. Howard. The kinesin-13 MCAK has an unconventional ATPase cycle adapted for microtubule depolymerization. *The European Molecular Biology Organization Journal*, 2011.

[27] K. Furuta, A. Furuta, Y. Y. Toyoshima, M. Amino, K. Oiwa, and H. Kojima. Measuring collective transport by defined numbers of processive and nonprocessive kinesin motors. *Biophysical Journal*, 2013.

[28] S. Gilbert, M. Moyer, and K. Johnson. Alternating site mechanism of the kinesin atpase. *Biochemistry*, 1998.

[29] S. Gilbert, M. Webb, M. Brune, and K. Johnson. Pathway of processive ATP hydrolysis by kinesin. *Nature*, 1995.

[30] D. Gillespie. Stochastic simulation of chemical kinetics. *Annual Review of Physical Chemistry*, 2007.

[31] A. J. Goldman, R. G. Cox, and H. Brenner. Slow viscous motion of a sphere parallel to a plane wall—i motion through a quiescent fluid. *Chemical engineering science*, 22(4):637–651, 1967.

[32] J. Goyette, C. S. Salas, N. Coker-Gordon, M. Bridge, S. A. Isaacson, J. Allard, and O. Dushek. Biophysical assay for tethered signaling reactions reveals tether-controlled activity for the phosphatase shp-1. *Science advances*, 2017.

[33] B. Grafstein and D. Forman. Intracellular transport in neurons. *Physiological Reviews*, 1980.

[34] B. J. Grant, R. A. Cross, and J. A. McCammon. Electrostatically biased binding of kinesin to microtubules. *Biophysical Journal*, 2011.

[35] S. Gross, M. Vershinin, and G. Shubeita. Cargo transport: two motors are sometimes better than one. *Current Biology*, 2007.

[36] L. Guillaud, S. El-Agamy, M. Otsuki, and M. Terenzio. Anterograde axonal transport in neuronal homeostatis and disease. *Frontiers in Molecular Neuroscience*, 2020.

[37] D. Hackney. Kinesin ATPase: rate-limiting ADP release. *Proceedings of the National Academy of Sciences*, 1988.

[38] D. Hackney and M. Stock. Kinesin's IAK tail domain inhibits initial microtubule-stimulated ADP release. *Nature Cell Biology*, 2000.

[39] J. Hammond, C. Huang, S. Kaech, C. Jacobson, G. Banker, and K. Verhey. Posttranslational modfications of tubulin and the polarized transport of kinesin-1 in neurons. *Molecular Biology of the Cell*, 2009.

[40] W. Hancock and J. Howard. Processivity of the motor protein kinesin requires two heads. *Journal of Cell Biology*, 1998.

[41] W. Hancock and J. Howard. Kinesin's processivty results from mechanical and chemical coordination between the ATP hydrolysis cycles of the two motor domains. *Proceedings of the National Academy of Sciences*, 1999.

[42] P. Hänggi, P. Talkner, and M. Borkovec. Reaction-rate theory: fifty years after kramers. *Reviews of modern physics*, 1990.

[43] P. Hill. Kernel estimation of a distribution function. *Communication in Statistics - Theory and Methods*, 1985.

[44] N. Hirokawa, K. Pfister, H. Yorifuji, M. Wagner, S. Brady, and G. Bloom. Submolecular domains of bovine brain kinesin identified by electron microscopy and monoclonal antibody decoration. *Cell*, 1989.

[45] P. Hooikaas, M. Martin, G. Kujnthes, C. Peeters, E. Katrukha, L. Ferrari, R. Stuchhi, D. Verhagen, W. van Riel, A. Altelaar, C. Hoogenraad, S. Rudiger, L. Kapitein, and A. Akhmanova. MAP7 family proteins are microtubule-tethered allosteric activators of kinesin-1. *Journal of Cell Biology*, 2019.

[46] C. Janke and M. Magiera. The tubulin code and its role in controlling microtubule properties and functions. *Nature Reviews: Molecular Cell Biology*, 2020.

[47] H. Jans, X. Liu, L. Austin, G. Maes, and Q. Huo. Dynamic light scattering as a powerful tool for gold nanoparticle bioconjugation and biomolecular binding studies. *Analytical Chemistry*, 2009.

[48] J. Kevenaar, S. Bianchi, M. van Spronsen, N. Olieric, J. Lipka, C. Frias, M. Mikhaylova, M. Harterink, N. Keijzer, P. Wulf, M. Hilbert, L. Kaptein, E. de Graaff, A. Ahkmanova, M. Steinmetz, and C. Hoogenraad. Kinesin-binding protein controls microtubule dynamics and cargo trafficking by regulating kinesin motor activity. *Current Biology*, 2016.

[49] P. Kloeden and P. E. Numerical solution of stochastic differential equations. *Springer*, 1992.

[50] S. Klumpp and R. Lipowsky. Cooperative cargo transport by several molecular motors. *Proceedings of the National Academy of Sciences*, 2005.

[51] H. Kojima, E. Muto, H. Higuchi, and T. Yanagida. Mechanics of single kinesin molecules measured by optical trapping nanometry. *Biophysical Journal*, 1997.

[52] Y. Konishi and M. Setou. Tubulin tyrosination navigates the kinesin-1 motor domain to axons. *Nature Neuroscience*, 2009.

[53] I. Kulic, A. Brown, H. Kim, and V. Gelfand. The role of microtubule movement in bidirectional organelle transport. *Proceedings of the National Academy of Sciences*, 2008.

[54] A. Kunwar, S. Tripathy, J. Xu, M. Mattson, P. Anand, R. Sigua, M. Vershinin, R. McKenney, C. Yu, A. Mogilner, and S. Gross. Mechanical stochastic tug-of-war models cannot explain bidirectional lipid-droplet transport. *Proceedings of the National Academy of Sciences*, 2011.

[55] M. L. Kutys, J. Fricks, and W. O. Hancock. Monte Carlo analysis of neck linker extension in kinesin molecular motors. *Public Library of Science Computational Biology*, 2010.

[56] M. Lakadamyali. Navigating the cell: how motors overcome roadbloacks and traffic jams to efficiently transport cargo. *Royal Society of Chemistry*, 2014.

[57] Y. Laurin, J. Eyer, C. Robert, C. Prevost, and S. Sacquin-Mora. Mobility and core-protein binding patterns of disordered C-terminal tails in β-tubulin isotypes. *Biochemistry*, 2017.

[58] C. Lawrence, R. Dawe, K. Christie, C. D.W., S. Dawson, S. Endow, L. Goldstein, G. H.V., N. Hirokawa, J. Howard, R. Malmberg, J. McIntosh, H. Miki, T. Mitchison, Y. Okada, A. Reddy, W. Saxton, M. Schliwa, J. Scholey, R. Vale, C. Walczak, and L. Wordeman. A standardized kinesin nomenclature. *The Journal of Cell Biology*, 2004.

[59] J. Leach, H. Mushfique, S. Keen, R. Di Leonardo, G. Ruocco, J. Cooper, and M. Padgett. Comparison of faxén's correction for a microsphere translating or rotating near a surface. *Physical Review E*, 79(2):026301, 2009.

[60] C. Leduc, O. Campàs, K. B. Zeldovich, A. Roux, P. Jolimaitre, L. Bourel-Bonnet, B. Goud, J.-F. Joanny, P. Bassereau, and J. Prost. Cooperative extraction of membrane nanotubes by molecular motors. *Proceedings of the National Academy of Sciences*, 2004.

[61] D. Lessard, O. Zinder, T. Hotta, and K. Verhey. Polyglutamylation of tubulin's c-terminal tail controls pausing and motility of kinesin-3 fmaily member kif1a. *Journal of Biological Chemistry*, 2019.

[62] Q. Li, S. King, A. Gopinathan, and J. Xu. Quantitative determination of the probability of multiple-motor transport in bead-based assays. *Biophysical Journal*, 2016.

[63] Q. Li, K.-F. Tseng, S. J. King, W. Qiu, and J. Xu. A fluid membrane enhances the velocity of cargo transport by small teams of kinesin-1. *Biophysical Journal*, 2018.

[64] W. Liang, Q. Li, K. Faysal, S. King, A. Gopinathan, and J. Xu. Microtubule defects influence kinesin-based transport in vitro. *Biophysical Journal*, 2016.

[65] J. Liepe, P. Kirk, S. Filippi, T. Toni, C. P. Barnes, and M. P. Stumpf. A framework for parameter estimation and model selection from experimental data in systems biology using approximate bayesian computation. *Nature protocols*, 2014.

[66] J.-M. Lueckmann, J. Boelts, D. Greenberg, P. Goncalves, and J. Macke. Benchmarking simulation-based inference. In *International conference on artificial intelligence and statistics*, 2021.

[67] L. Mabonga and A. Kappo. Protein-protein interaction modulators: advances, succeses and remaining challenges. *Biophysical Reviews*, 2019.

[68] S. Marbach and C. E. Miles. Coarse-grained dynamics of transiently bound fast linkers. *The Journal of Chemical Physics*, 2023.

[69] K. Mickolajczyk, N. Deffenbaugh, J. Ortega Arroyo, and W. Hancock. Kinetics of nucleotide-dependent structural transitions in the kinesin-1 hydrolysis cycle. *Proceedings of the National Academy of Sciences*, 2015.

[70] H. Miki, Y. Okada, and N. Hirokawa. Analysis of the kinesin superfamily: insights into structure and function. *Trends in Cell Biology*, 2005.

[71] C. Miles and J. Keener. Bidirectionality from cargo thermal fluctuations in motor-mediated transport. *Journal of Theoretical Biology*, 2017.

[72] C. Miles, S. Lawley, and J. Keener. Analysis of nonprocessive molecular motor transport using renewal reward theory. *Society for Industrial and Applied Mathematicians Journal on Applied Mathematics*, 2018.

[73] B. Milic, J. Andreasson, W. Hancock, and S. Block. Kinesin processivity is gated by phosphate release. *Proceedings of the National Academy of Sciences*, 2014.

[74] S. Mogre, J. Christensen, S. Reck-Peterson, and E. Koslover. Optimizing microtubule arrangements for rapid cargo capture. *Biophysical Journal*, 2021.

[75] G. Morfini, M. Burns, L. Binder, N. Kanaan, N. LaPointe, D. Bosco, R. Brown Jr., H. Brown, A. Tiwari, L. Hayward, J. Edgar, K. Nave, J. Garberrn, Y. Atagi, Y. Song, G. Pigino, and S. Brady. Axonal transport defects in neurodegenerative diseases. *Journal of Neuroscience*, 2009.

[76] V. C. Nadar, A. Ketschek, K. A. Myers, G. Gallo, and P. W. Baas. Kinesin-5 is essential for growth-cone turning. *Current Biology*, 2008.

[77] W. Nam and B. Epureanu. Highly loaded behavior of kinesins increases the robustness of transport under high resisting loads. *Public Library of Science Computational Biology*, 2015.

[78] A. Nicolas, K. Kenna, A. Renton, N. Ticozzi, F. Faghri, R. Chia, and et al. Genome-wide analyses identify KIF5A as a novel ALS gene. *Neuron*, 2018.

[79] T. Nishizaka, H. Miyata, H. Yoshikawa, S. Ishiwata, and K. Kinosita Jr. Unbinding force of a single motor molecule of muscle measured using optical tweezers. *Nature*, 1995.

[80] E. Nogales, S. Wolf, and K. Downing. Structure of the alpha beta tublin dimer by electron crystallography. *Nature*, 1998.

[81] K. M. Ori-McKenney and R. J. McKenney. Tau oligomerization on microtubules in health and disease. *Cytoskeleton*, 2023.

[82] H. Palacci, O. Idan, M. J. Armstrong, A. Agarwal, T. Nitta, and H. Hess. Velocity fluctuations in kinesin-1 gliding motility assays originate in motor attachment geometry variations. *Langmuir*, 2016.

[83] A. Pan, A. Pan, B. Brooks, and X. Wu. Molecular simulation study on the walking mechanism of kinesin dimers on microtubules. *Current Advances in Chemistry and Biochemistry*, 2021.

[84] L. Popovic, S. McKinley, and M. Reed. A stochastic compartmental model for fast axonal transport. *Society for Industrial and Applied Mathematicians Journal on Applied Mathematics*, 2011.

[85] C. L. Porter, S. L. Diamond, T. Sinno, and J. C. Crocker. Shear-driven rolling of dna-adhesive microspheres. *Biophysical Journal*, 120(11):2102–2111, 2021.

[86] H. Rafii-Tabar and R. Tavakoli-Darestani. Modelling the stochastic dynamics of biological nano-motors: an overview of recent results. *Journal of Computational and Theoretical Nanoscience*, 2009.

[87] C. Rakers, M. Bermudez, B. G. Keller, J. Mortier, and G. Wolber. Computational close up on protein–protein interactions: how to unravel the invisible using molecular dynamics simulations? *Wiley Interdisciplinary Reviews: Computational Molecular Science*, 2015.

[88] B. Reddy, N. Allipeta, and S. Gross. A new method to experimentally quantify dynamics of protein-protein interactions. *accepted to Communications Biology*, 2023.

[89] B. Reddy, S. Tripathy, M. Vershinin, M. Tanenbaum, J. Xu, M. Mattson-Hoss, K. Arabi, D. Chapman, T. Doolin, C. Hyeon, and S. P. Gross. Heterogeneity in kinesin function. *Traffic*, 2017.

[90] N. Reed, D. Cai, G. Blasius, E. Jih, E. Meyhofer, J. Gaertig, and K. Verhey. Microtubule acetylation promotes kinesin-1 binding and transport. *Current Biology*, 2006.

[91] E. Reid, M. Kloos, A. Ashley-Koch, L. Hughes, S. Bevan, I. Svenson, and et al. A kinesin heavy chain(KIF5A) mutation in hereditary spastic paraplegia (SPG10). *American Journal of Human Genetics*, 2002.

[92] G. Saper and H. Hess. Synthetic systems powered by biological molecular motors. *Chemical reviews*, 2019.

[93] N. Sarpangala and A. Gopinathan. Cargo surface fluidity can reduce inter-motor mechanical interference, promote load-sharing and enhance processivity in teams of molecular motors. *Public Library of Science Computational Biology*, 2022.

[94] M. Sataric, D. Sekulic, S. Zdravkovic, and N. Ralevic. A biophysical model of how α tubulin carboxy-terminal tails tune kinesin-1 processivity along microtubule. *Journal of Theoretical Biology*, 2017.

[95] W. Schief, R. Clark, and A. Crevenna. Inhibition of kinesin motility by ADP and phosphate supports a hand-over-hand mechanism. *Proceedings of the National Academy of Sciences*, 2004.

[96] G. Schreiber, G. Haran, and H.-X. Zhou. Fundamental aspects of protein- protein association kinetics. *Chemical reviews*, 2009.

[97] G. Schreiber and A. E. Keating. Protein binding specificity versus promiscuity. *Current opinion in structural biology*, 2011.

[98] A. Seitz, H. Kojima, K. Oiwa, E. M. Mandelkow, Y. H. Song, and E. Mandelkow. Single-molecule investigation of the interference between kinesin, Tau and MAP2c. *The European Molecular Biology Organization Journal*, 2002.

[99] X.-X. Shi, Y.-B. Fu, S.-K. Guo, P.-Y. Wang, H. Chen, and P. Xie. Investigating role of conformational changes of microtubule in regulating its binding affinity to kinesin by all-atom molecular dynamics simulation. *Proteins: Structure, Function, and Bioinformatics*, 2018.

[100] T. Shimizu and et al. Expression, purification, ATPase properties, and microtubule-binding properties of the ncd motor domain. *American Chemistry Society*, 1995.

[101] T. Shimizu, K. Thorn, A. Ruby, and R. Vale. ATPase kinetic characterization and single molecule behavior of mutant human kinesin motors defective in microtubule-based motility. *American Chemistry Society*, 2000.

[102] M. Sirajuddin, L. Rice, and R. Vale. Regulation of microtubule motors by tubulin isotypes and post-translational modifications. *Nature Cell Biology*, 2014.

[103] S. Sisson, Y. Fan, and M. Tanaka. Sequential Monte Carlo without likelihoods. *Proceedings of the National Academy of Sciences*, 2007.

[104] H. Sosa, E. Peterman, W. Moerner, and L. Goldstein. ADP-induced rocking of the kinesin motor domain revealed by single-molecule fluorescence polarization microsopy. *Nature Structural Biology*, 2001.

[105] U. Sotaro and S. Ishiwata. Loading direction regulates the affinity of ADP for kinesin. *Nature Structural and Molecular Biology*, 2003.

[106] B. Sprinkle, E. B. Van Der Wee, Y. Luo, M. M. Driscoll, and A. Donev. Driven dynamics in dense suspensions of microrollers. *Soft Matter*, 2020.

[107] A. Szabo, K. Schulten, and Z. Schulten. First passage time approach to diffusion controlled reactions. *The Journal of chemical physics*, 1980.

[108] N. Tajielyato, L. Li, Y. Peng, J. Alper, and E. Alexov. E-hooks provide guidance and a soft landing for the microtubule binding domain of dynein. *Scientific Reports*, 2018.

[109] K. Thorn, J. Ubersax, and R. Vale. Engineering the processive run length of the kinesin motor. *Journal of Cell Biology*, 2000.

[110] I. Tikhonenko, V. Magidson, R. Gräf, A. Khodjakov, and M. P. Koonce. A kinesin-mediated mechanism that couples centrosomes to nuclei. *Cellular and Molecular Life Sciences*, 2013.

[111] K. Titeca, I. Lemmens, J. Tavernier, and S. Eyckerman. Discovering cellular protein-protein interactions: technological strategies and opportunities. *Mass Spectrometry Reviews*, 2018.

[112] A. Toleikis, N. Carter, and R. Cross. Backstepping mechanism of kinesin-1. *Biophysical Journal*, 2020.

[113] S. Uemura, K. Kawaguchi, J. Yajima, M. Edamatsu, Y. Y. Toyoshima, and S. Ishiwata. Kinesin–microtubule binding depends on both nucleotide state and loading direction. *Proceedings of the National Academy of Sciences*, 2002.

[114] R. Vale and R. Fletterick. The design plan of kinesin motors. *Annual Review of Cell and Developmental Biology*, 1997.

[115] K. Verhey and J. Hammond. Traffic control: regulation of kinesin motors. *Nature Reviews: Molecular Cell Biology*, 2009.

[116] M. Vershinin, B. Carter, D. Razafsky, S. King, and S. Gross. Multiple-motor based transport and its regulation by tau. *Proceedings of the National Academy of Sciences*, 2007.

[117] J. Vickers, A. King, A. Woodhouse, M. Kirkcaldie, J. Staal, G. McCormack, C. Blizzard, R. Musgrove, S. Mitew, Y. Liu, J. Chuckowree, O. Bibari, and T. Dickson. Axonopathy and cytoskeletal disruption in degenerative diseases of the central nervous system. *Brain Research Bulletin*, 2009.

[118] K. Wall, H. Hart, T. Lee, C. Page, T. Hawkins, and L. Hough. C-terminal tail polyglycylation and polyglutamylation alter microtubule mechanical properties. *Biophysical Journal*, 2020.

[119] Q. Wang, J. Tian, H. Chen, H. Du, and L. Guo. Amyloid beta-mediated KIF5A deficiency disrupts anterograde axonal mitochondrial movement. *Neurobiology of Disease*, 2019.

[120] D. J. Warne, R. E. Baker, and M. J. Simpson. Rapid bayesian inference for expensive stochastic models. *Journal of Computational and Graphical Statistics*, 2022.

[121] O. Wattanathamsan and P. Varisa. Post-translational modifications of tubulin: their role in cancers and the regulation of signaling molecules. *Cancer Gene Therapy*, 2023.

[122] L. Wordeman. How kinesin motor proteins drive mitotic spindle function: Lessons from molecular assays. In *Seminars in Cell & Developmental Biology*, 2010.

[123] J. Xu, Z. Shu, S. J. King, and S. P. Gross. Tuning multiple motor travel via single motor velocity. *Traffic*, 2012.

[124] C. Xue, B. Shtylla, and A. Brown. A stochastic multiscale model that explains the segregration of axonal microtubules and neurofilaments in neuological diseases. *Public Library of Science Computational Biology*, 2015.

[125] S. Yadav and A. Kunwar. Sliding of motor tails on cargo surface due to drift and diffusion affects their team arrangement and collective transport. *Physical Biology*, 2022.

[126] W. Yan, S. Ansari, A. Lamson, M. A. Glaser, R. Blackwell, M. D. Betterton, and M. Shelley. Toward the cellular-scale simulation of motor-driven cytoskeletal assemblies. *Elife*, 2022.

[127] A. Yildiz, M. Tomishige, R. Vale, and S. P. Kinesin walks hand-over-hand. *Science*, 2004.

[128] T. Zaniewski and W. Hancock. The net charge of the k-loop regulates KIF1A superprocessivity by enhancing microtubule affinity in the one-head-bound state. *bioRxiv*, 2022.

[129] P. Zhang. Model selection via multifold cross validation. *The annals of statistics*, 1993.

[130] Z. Zhang, N. Danne, B. Meddens, and J. Erwin. Direct imaging of intraflagellar-transport turnarounds reveals that motors detach, diffuse, and reattach to opposite-direction trains. *Proceedings of the National Academy of Sciences*, 2021.

[131] Z. Zhang, Y. Goldtzvik, and D. Thirumalai. Parsing the roles of neck-linker docking and tethered head diffusion in the stepping dynamics of kinesin. *Proceedings of the National Academy of Sciences*, 2017.

[132] H.-X. Zhou and P. A. Bates. Modeling protein association mechanisms and kinetics. *Current opinion in structural biology*, 2013.

Appendix A

Chapter 2 Supplementary Materials

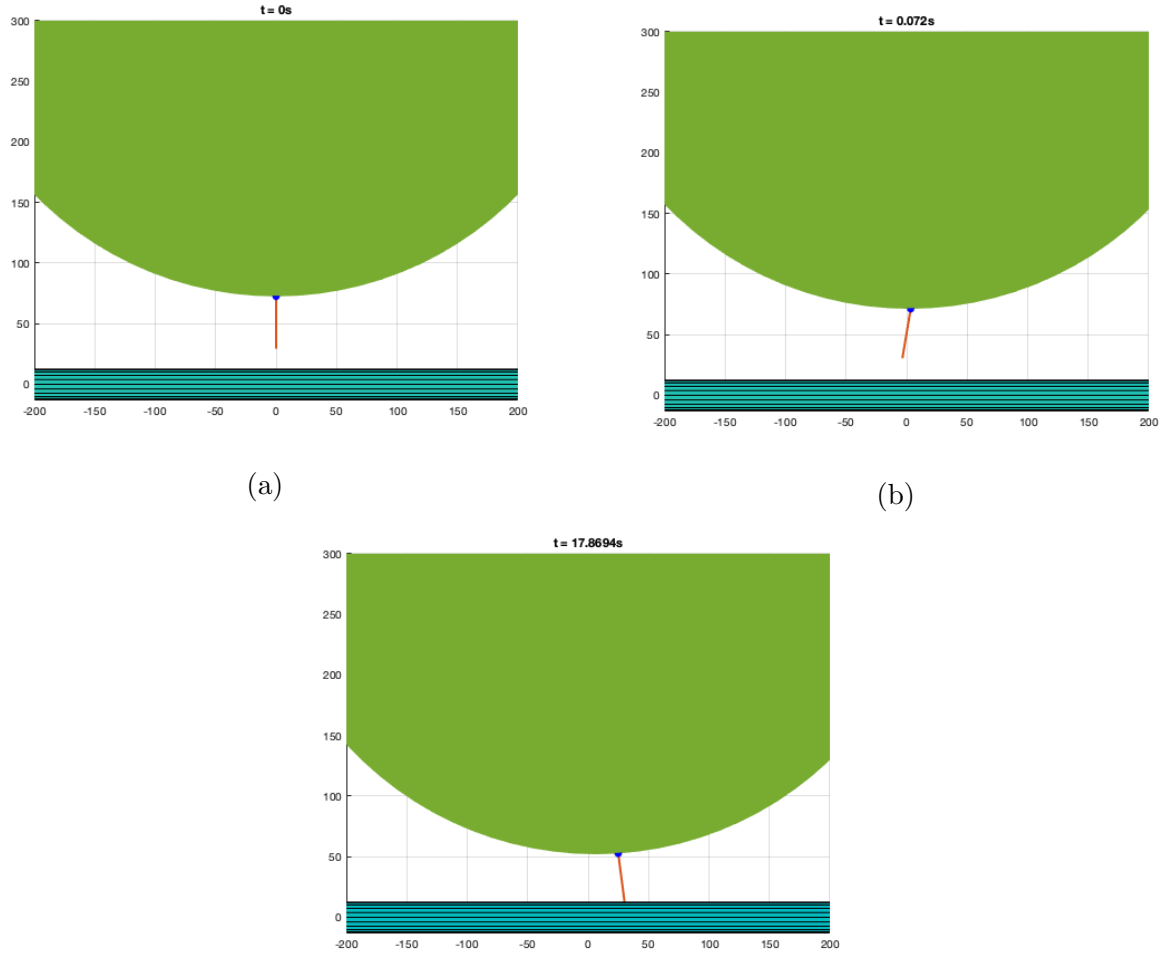

(a)

(b)

(c)

Figure A.1: **Simulation Snapshots.** The simulation starts as in (a), where the motor (red line) is anchored (blue dot) to the bottom of the cargo (green sphere). The microtubule (turquoise cylinder) is centered at (0,0), and the axes depict locations of other components with respect to the microtubule center, in nanometers. As the simulation continues, the cargo and the motor diffuses with respect to force laws (b). The simulation ends when the motor strongly binds to the microtubule (c). Time (seconds) at which each event occurs is shown above figures.

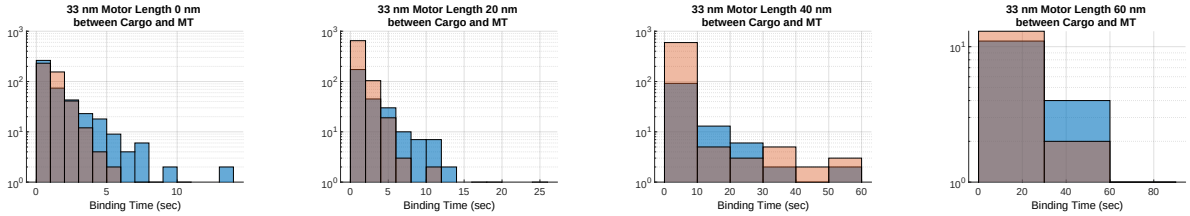

(a) (b) (c) (d)

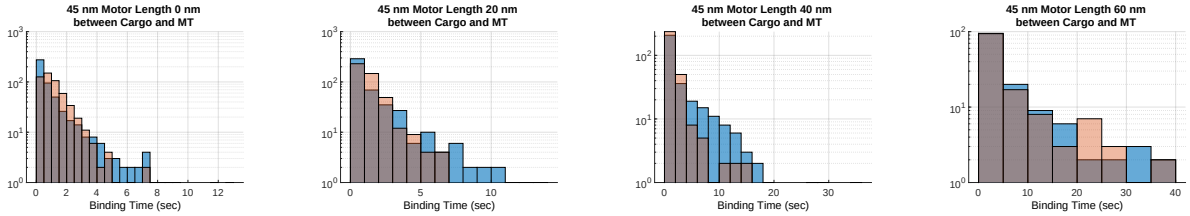

(e) (f) (g) (h)

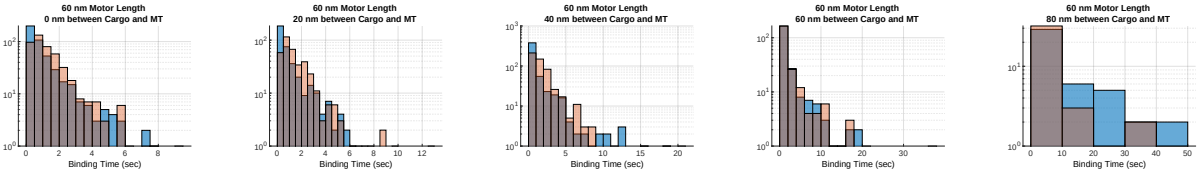

(i) (j) (k) (l) (m)

Figure A.2: **Full distributions of binding times.** Simulated data from ADP release model (red) is plotted over experimental data (blue). Overlap between distributions is shown in grey.

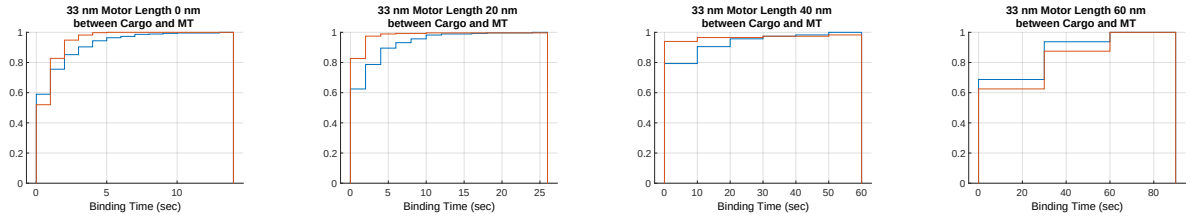

(a) (b) (c) (d)

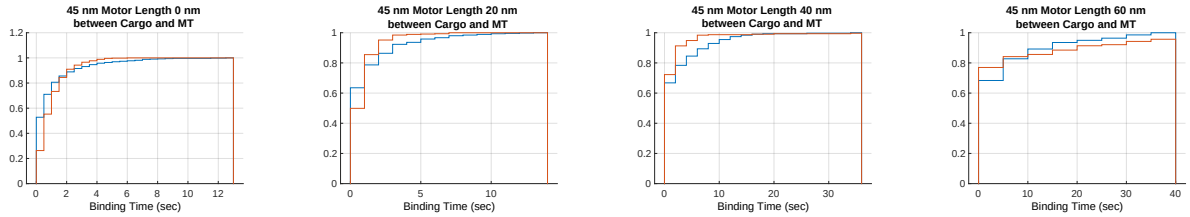

(e) (f) (g) (h)

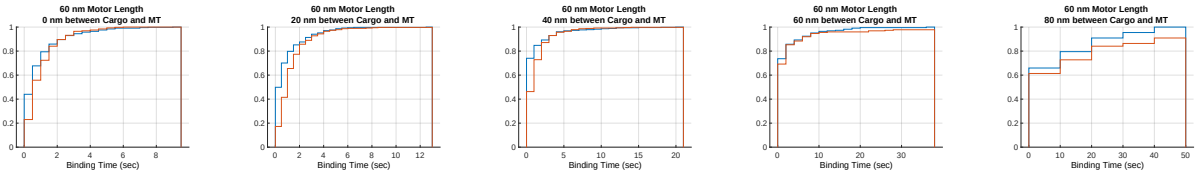

(i) (j) (k) (l) (m)

Figure A.3: **Cumulative distributions of binding times.** Simulated data from ADP release model (red) is plotted over experimental data (blue). Same information as Figure A.2 but CDF instead of PDF.

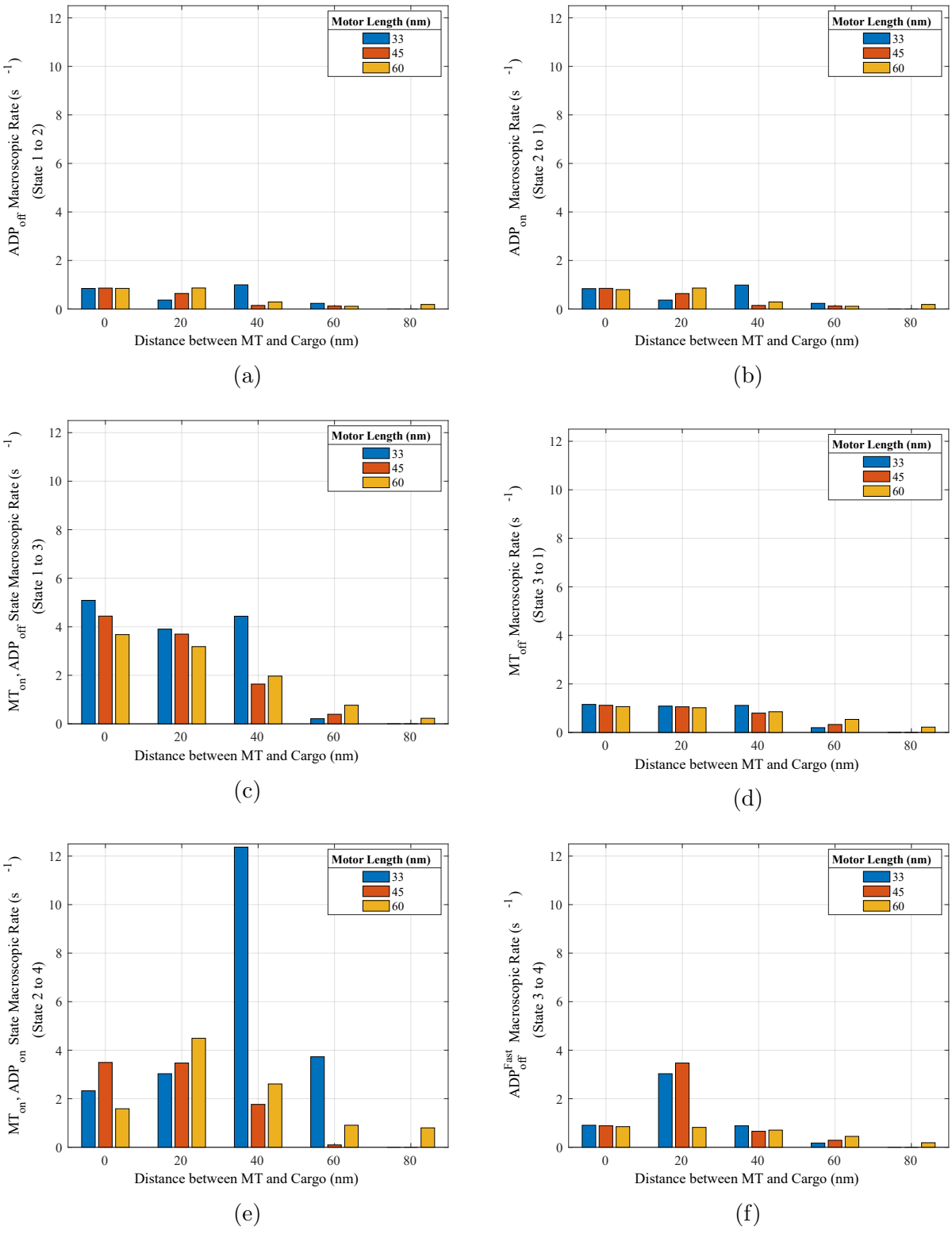

Figure A.4: **Macroscopic rates of state transitions.** Rates for each transition in the ADP+Diffusion model estimated with respect to average distance between the microtubule and the cargo for each motor length. Parameters from Table 2.1 were used.

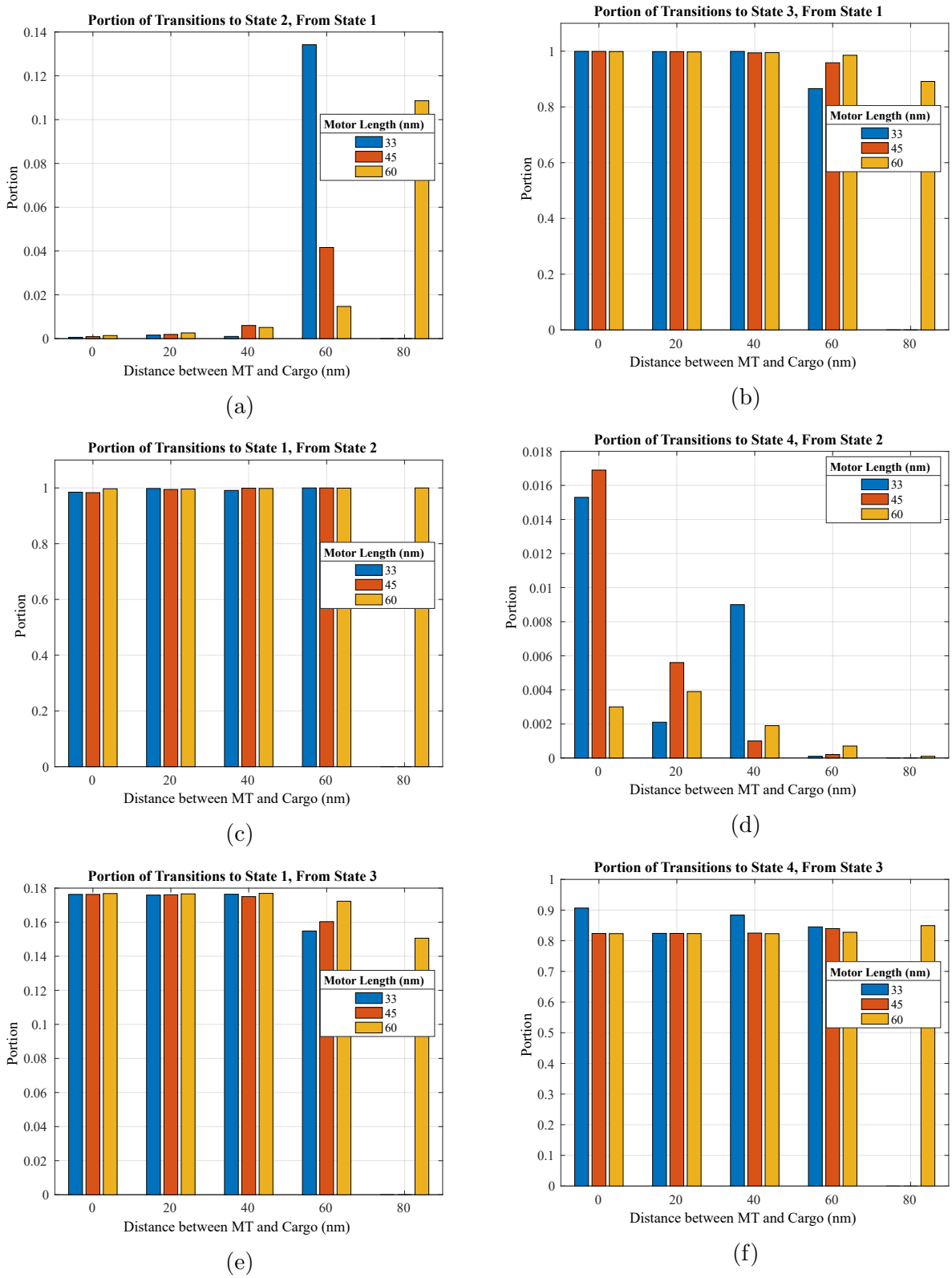

Figure A.5: **Proportion of Transitions**. Of the two possible transitions *out* of each state, the relative proportions are shown. Parameters from Table 2.1 were used.

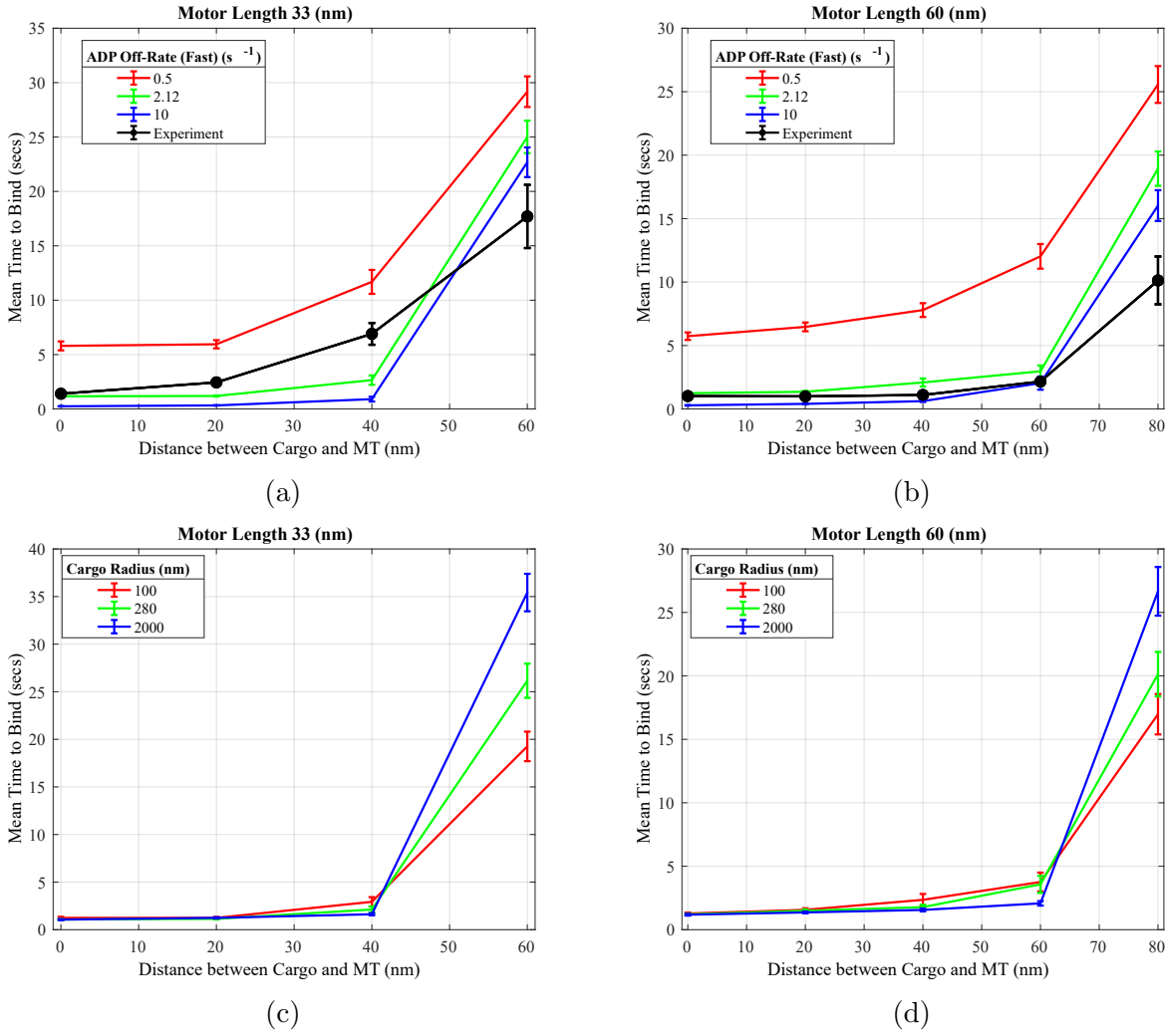

Figure A.6: **Other Parameter Sweeps on Binding Times.** $k_{\text{off}}^{\text{ADP,Fast}}$ (a-b) and cargo size (c-d) were varied in the ADP release model. Data are presented as mean ± SEM.

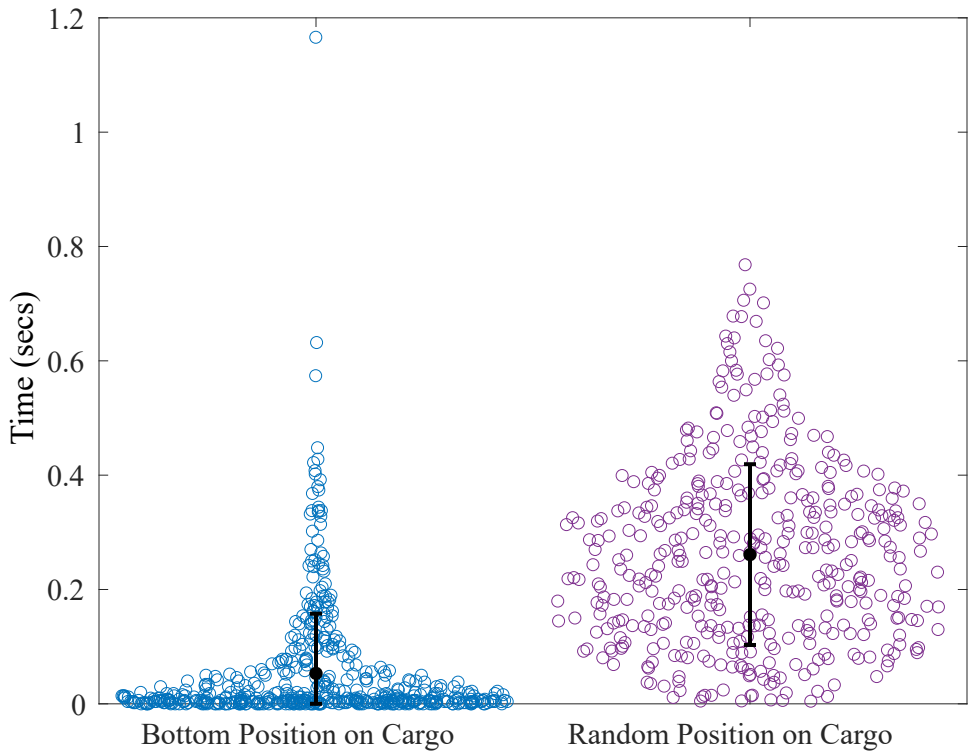

Figure A.7: **Cargo Rotation Time.** The motor anchor's initial position on the cargo is either fixed at the bottom of the cargo (left) or randomized (right), and the time for the motor to perform a diffusive search of the microtubule was simulated. $n = 500$.

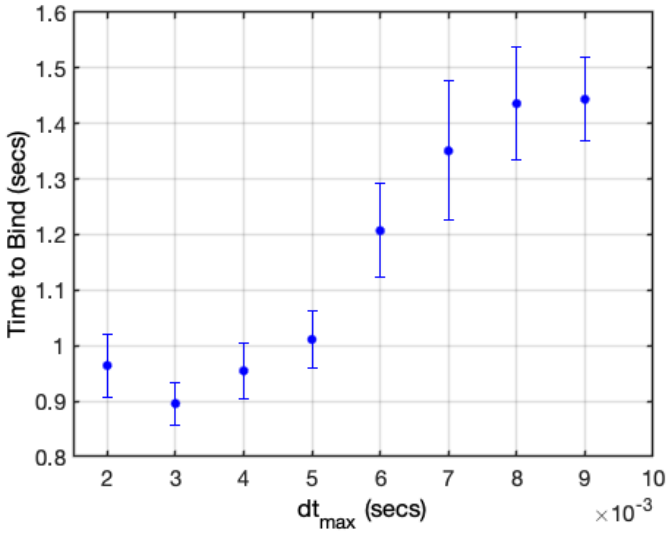

Figure A.8: **Time step convergence study**. Maximum time step was varied and converged to a common binding time. 0.004 was the largest maximum time step that resulted in a binding time that is relatively similar to the results from smaller maximum time step. $n = 1000$.

Table A.1: Posterior Density Method Validation. Simulated data was generated using the ADP release model and the Simulated Values. A sequential Monte Carlo approximate Bayesian computational algorithm was performed on the fake data and recovered the simulated values (Estimated Value).

Parameter	Simulated Value	Estimated Value
$k_{\text{off}}^{\text{ADP}}$	0.8	0.78
$k_{\text{on}}^{\text{ADP}}$	1000	1021.3
$k_{\text{off}}^{\text{ADP,Fast}}$	6.3	6.22
$k_{\text{on}}^{\text{MT}}$	10	9.83
$k_{\text{off}}^{\text{MT}}$	1	0.89
D_m	1000	987.56
κ_w	0.005	0.0057

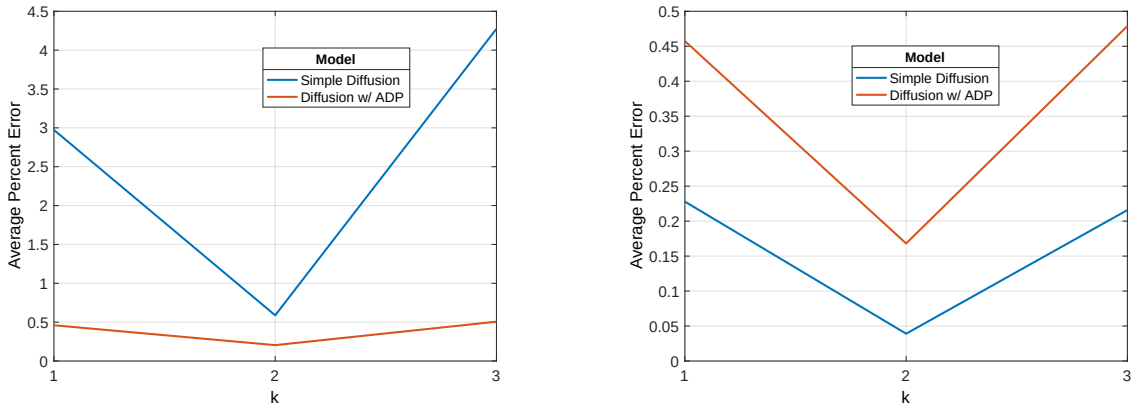

(a) Synthetic data from ADP release model (b) Synthetic data from Simple Diffusion model

Figure A.9: **Cross-Validation Test**. Synthetic data was simulated using either the ADP release model (a) or the Simple Diffusion model (b), and both the ADP release and the Simple Diffusion models' performance were evaluated using k-fold cross-validation.

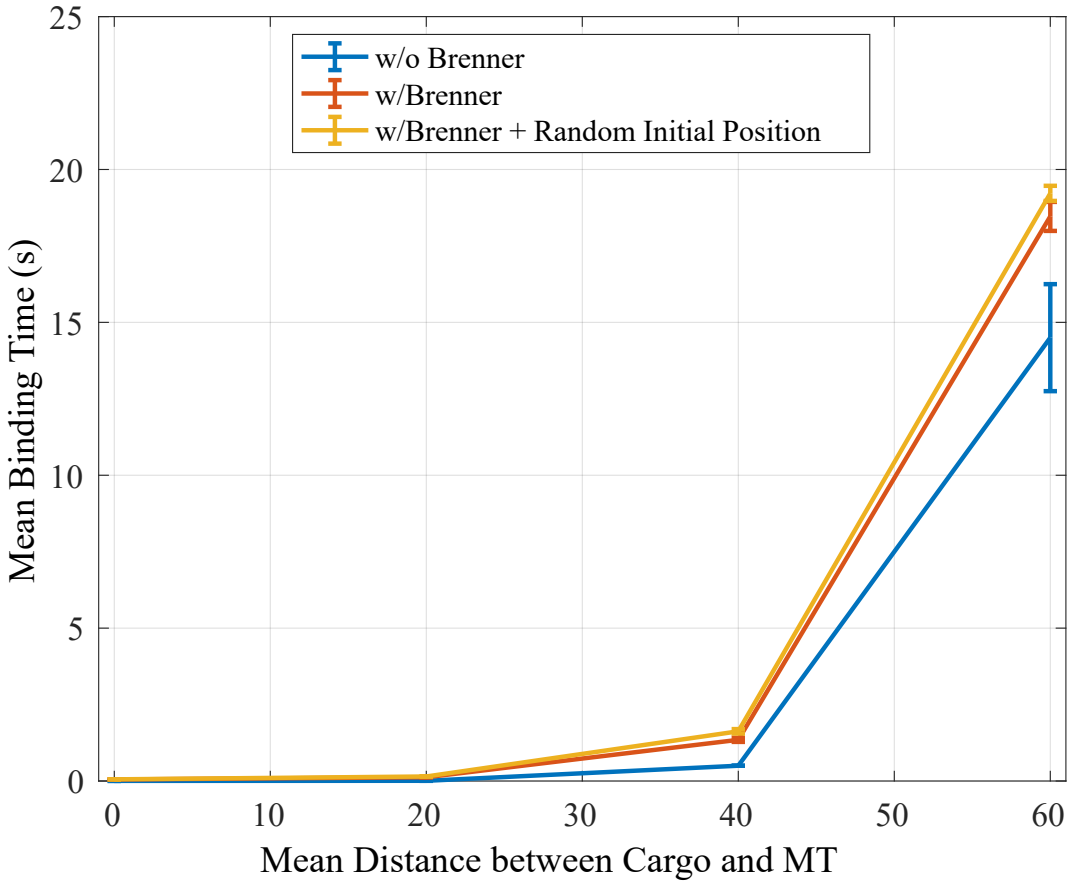

Figure A.10: Impact of Hydrodynamic Effects On Binding Time. To investigate the role of hydrodynamic near-wall effects, we modified the rotational and translational diffusion coefficients by their z-dependent orthogonal corrections via the classical Brenner formulae, neglecting the parallel-to-wall asymmetry as an approximation. The blue curve without correction shows the same prediction as the main text diffusion model for 33 nm motors. The red curve adds the Brenner correction, showing a slight increase in binding time at far distances. To further magnify the effect, random starting orientations (yellow) of the cargo add additional slowdown with hydrodynamics but fail to explain the short distance delays.

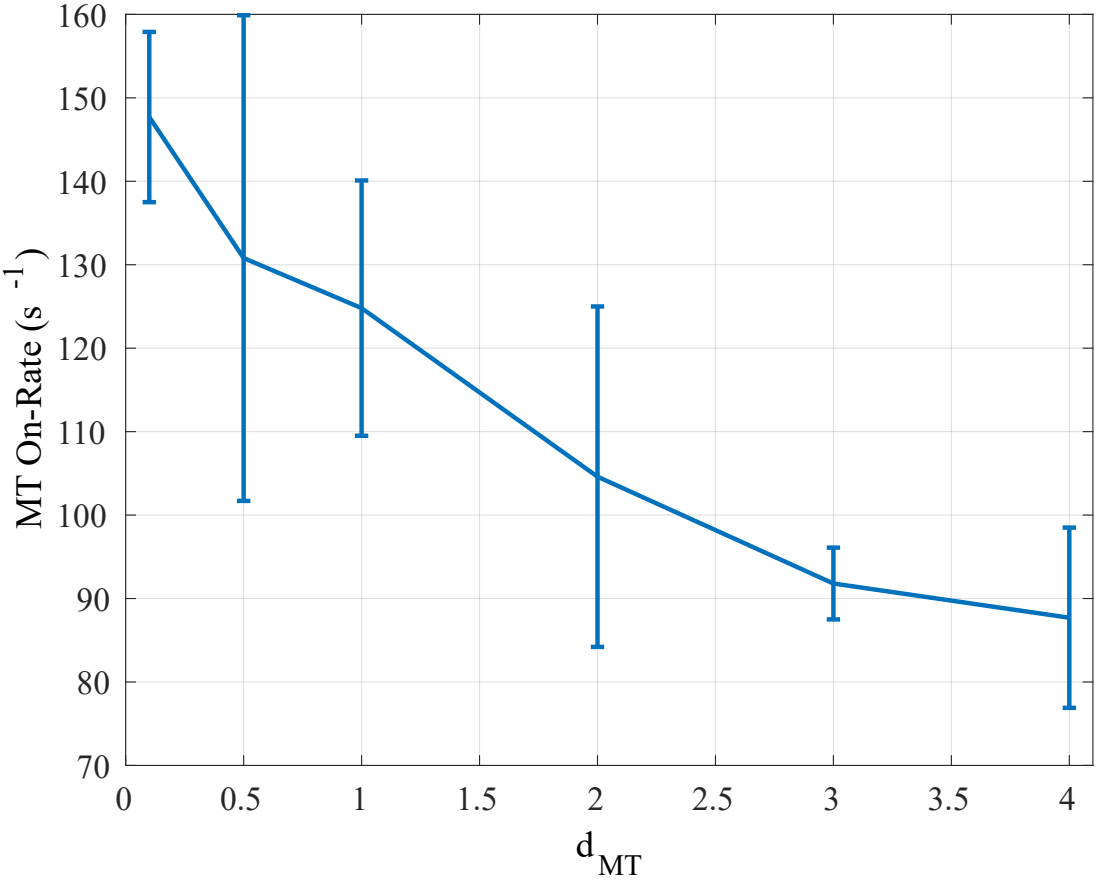

Figure A.11: Role of Motor-Microtubule Binding Radius in Fitting. To investigate how changing the binding radius d_{MT} affects inferred parameter values, we sweep over ranges smaller and larger than the one considered in the main text (5 nm) and fit the full model on all 3 motor lengths. As d_{MT} becomes smaller, k_{MT} becomes larger, but remains on the same order of $\approx 100\mathrm{s}^{-1}$. Over this range, cumulative absolute fitting errors differed at most 0.01s.

Appendix B

Chapter 3 Supplementary Materials

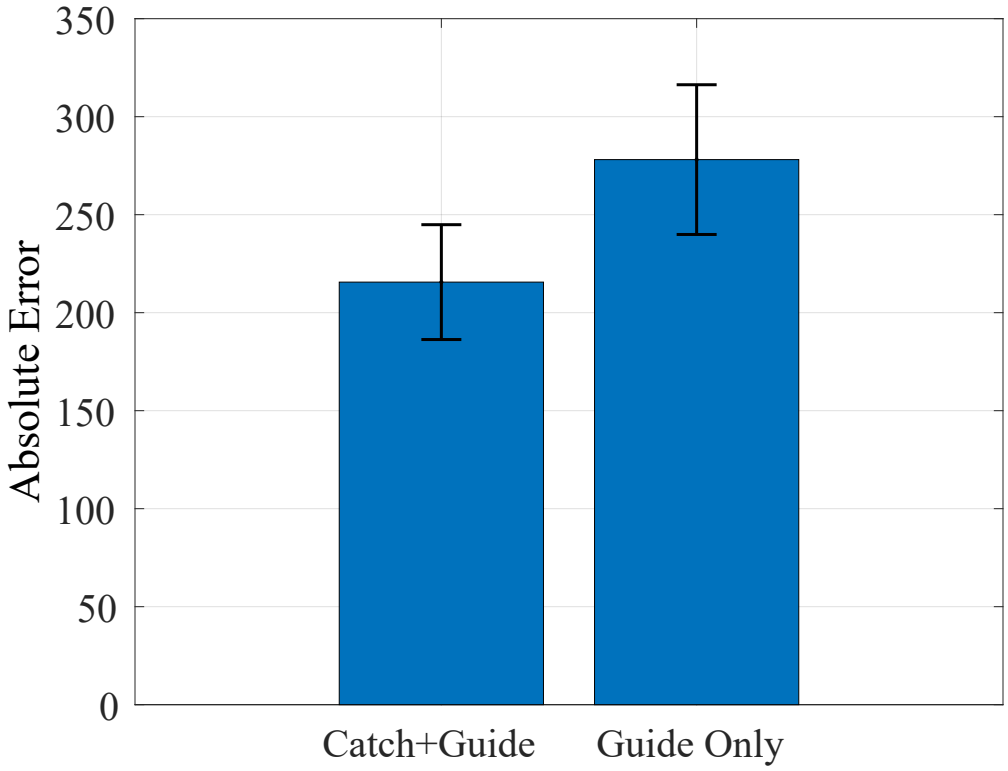

Figure B.1: Both models were trained on experimental velocity data and subsequently tested on processivity. Absolute error between the predicted and experimental processivity is presented as mean ± SEM. Predictive performance of both models were not significantly different from each other ($p = 0.43$).

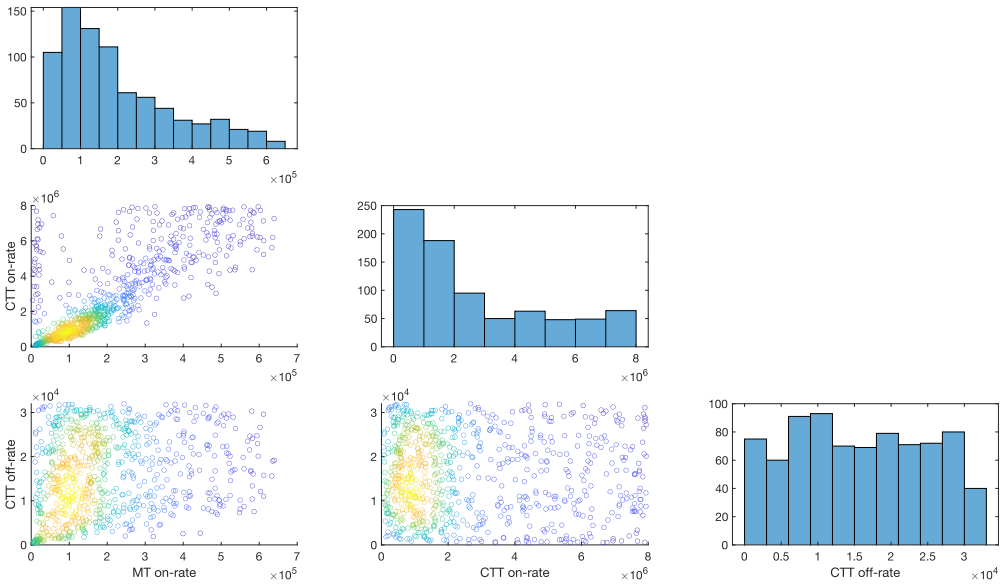

Figure B.2: Inference was performed on the CTT-stimulating-ADP-release model using a simple approximate Bayesian computation method. The parameters that resulted in the lowest 1% absolute error between simulation and experimental data from wildtype microtubules were chosen.